Title: Neuroendocrine cells initiate protective upper airway reflexes

Authors: Laura F. Seeholzer[1]* and David Julius[1]*

Affiliations:

[1]Department of Physiology, University of California, San Francisco; San Francisco, 94143, USA.

*Corresponding authors. Emails: laura.seeholzer@ucsf.edu; david.julius@ucsf.edu

Abstract: Airway neuroendocrine (NE) cells have been proposed to serve as specialized sensory epithelial cells that modulate respiratory behavior by communicating with nearby nerve endings. However, their functional properties and physiological roles in the healthy lung, trachea and larynx remain largely unknown. Here, we show that NE cells in these compartments possess distinct biophysical properties, but share sensitivity to the commonly aspirated noxious stimuli, water and acid. Moreover, we found that tracheal and laryngeal NE cells protect the airways by releasing ATP to activate purinoreceptive sensory neurons that initiate swallowing and expiratory reflexes. Our work uncovers striking molecular and biophysical diversity of NE cells across the airways and reveals mechanisms by which these specialized excitable cells serve as sentinels for activating a critical nociceptive circuit.

Main Text:
The respiratory tract must guard against inhalation of noxious agents such as food, liquid, or corrosive acid from gastric reflux. Airway protection is mediated by reflexes like cough, swallowing or apneas. Dysfunction of these reflexes promotes aspiration of foreign entities into the lung, which is a major cause of morbidity and mortality across demographics and clinical settings (*1–4*). Our airways are densely innervated by sensory nerve fibers, which can detect relevant stimuli to drive these protective reflexes (*5–8*). However, stimulus detection may also be mediated by specialized sensory epithelial cells that activate neural circuits regulating behavior, as occurs in other organs such as the gut and tongue (*8–11*). In the airways, one putative sensory cell type that resides in close proximity to nerve fibers is the neuroendocrine (NE) cell (*12*), a rare, specialized epithelial cell whose functional properties and roles under normal physiologic conditions remain poorly characterized.

NE cells have been studied mostly for their proliferative potential following airway injury (*13–15*). Pulmonary NE cells, a subtype that resides in the intrapulmonary airways, also have important roles in type II immune responses (*16–19*) and small cell lung cancer (*20, 21*). While pulmonary NE may detect multimodal stimuli (*22–28*), their functional properties are relatively unknown compared to sensory epithelial cells in other organs. Even less is known about the sensory properties and functions of NE cells in more proximal airways such as the trachea and larynx. To understand the contributions of NE cells to stimulus detection, physiology, and behavior, we characterized and compared their biophysical and functional properties within each of these airway compartments. We show that NE cells are excitable and exhibit distinct characteristics along the airway axis. Specifically, we demonstrate that NE cells in the lung are mechanically sensitive, whereas those in the larynx and trachea respond primarily to noxious aspiration-related stimuli. Furthermore, we show that laryngeal and tracheal NE cells release purinergic transmitters onto neighboring primary afferent neurons and demonstrate that functional communication between these two excitable cell types is necessary and sufficient to drive protective reflexes.

Molecular and functional diversity of NE cells across the airway
Ascl1 is a lineage-defining transcription factor for NE cells (*29*), enabling us to use *Ascl1*^{CreERT2}; *R26*$^{LSL-tdTomato}$ mice to label and isolate NE cells from the lung, trachea and, to our surprise, a novel population in the larynx (Fig. 1A, Fig. S1A), (*18, 30*). Indeed, histological and transcriptomic analyses showed that *Ascl1*^{CreERT2} selectively and comprehensively labels neuroendocrine cells throughout the airways (fig. S1A-C).

Murine NE cells exhibit molecular and morphological differences across the airways (Fig. 1A-C, fig. S1D-H), (*30*). For example, pulmonary NE cells are rounded and form clusters (*12*), while tracheal and laryngeal NE cells are exclusively solitary with snout-like luminal projections (Fig. 1A-C). Interestingly, all human NE cells in healthy airways, including pulmonary NE cells, assume this solitary organization and distinctive morphology (Fig. 1B), (*15, 30–32*). We also noted differences in signaling molecules across populations. Pulmonary NE cells were enriched for osteopontin (*Spp1*) and cocaine- and amphetamine-regulated transcript (*Cartpt*), while tracheal and laryngeal NE cells were enriched for the B cell chemoattractant *Cxcl13* (fig. S1D) (*22, 33*). Moreover, only a subset of tracheal and laryngeal NE cells expressed CGRP or serotonin, whereas all pulmonary NE cells were CGRP-positive and serotonergic (fig. S1E-H). NE cells throughout the airways were seen to reside in close apposition to nerve fibers. Moreover, they were strikingly dense in the larynx, but gradually sparser in more distal airways (Fig. 1C, D, fig. S1I), mirroring relative nerve fiber innervation.

In sensory cells, intrinsic electrical properties can determine spontaneous activity, stimulus thresholds for synaptic release, and signal transduction dynamics. Using patch-clamp electrophysiology (fig. S2A), we found that NE cells had distinct biophysical properties in different regions of the airway. Unlike pulmonary NE cells, which only ever fired a single action potential, trachea/laryngeal NE cells were capable of spontaneous activity and firing action potential trains (Fig. 1E, F, Movie S1). Likewise, while inward currents in all NE cell subtypes were driven primarily by tetrodotoxin (TTX)-sensitive voltage-gated sodium (Na_V) channels, these currents were significantly larger in tracheal and laryngeal NE cells, as was expression of Na_V channel transcripts (Fig. 1G, fig. S2B-G). When we used a previously recorded action potential train as a voltage stimulus, we found that multi-spiking (but not mono-spiking) tracheal NE cells displayed Na_V current with each action potential (fig. S2H) and had larger Na_V currents (fig. S2I). Together, these data suggest a molecular basis for differential excitability, since increases in Na_V currents are known to enhance firing rate (*34*). In all NE cells, outward currents were driven primarily by TEA-sensitive voltage-gated potassium (K_V) channels (~80% of current, fig. S3A-H), with the remaining TEA-insensitive current likely due to two-pore potassium channels (fig. S3F, I)(*35*). Tracheal and laryngeal NE cells had significantly larger K_V current compared to pulmonary NE cells (Fig. 1G), but no significant difference was seen between mono- and multi-spiking tracheal NE cells (fig. S2I), suggesting that increased hyperpolarization does not account for differences in spiking profile. Importantly, whole-cell patch-clamp recordings from pulmonary and tracheal NE cells in intact tissue similarly showed that only tracheal/laryngeal NE cells fired multiple action potentials and had greater Na_V and K_V currents (Fig. 1H, I).

To determine if action potentials drive calcium influx, which can coordinate neurotransmitter release (*36*), we carried out simultaneous patch-clamp recording and calcium imaging from dissociated NE cells expressing the genetically encoded calcium indicator GCaMP5 (*Ascl1*[CreERT2]; *Polr2a*[LSL-GCaMP5G, tdTomato]). For all NE cell types, calcium influx was time-locked with current-evoked or spontaneous action potentials (Fig. 1J, fig. S4A, B). Furthermore, we found that the NE cells express T-type voltage gated calcium channels as high-potassium (high-k) evoked activity was blocked specifically by T-type inhibitors (Mibefradil and NNC 55-0396, fig. S4C, D) and stepping the NE cell's holding potential to -35 mV (which should uniquely activate T-type channels) elicited calcium influx (fig. S4E). Taken together, our data show that NE cells share common features, but also exhibit striking morphological and biophysical differences across the airway, suggesting distinct physiological functions and mechanisms for processing environmental stimuli.

Differential mechanical sensitivity of lower and upper airway NE cells
The mechanosensitive ion channel *Piezo2* was enriched in pulmonary NE cells (fig. S5A) and although mechanical sensitivity of NE cells has been inferred (*37, 38*), it has not been directly demonstrated. We found that mechanical stimulation indeed elicited Piezo2-like rapidly adapting inward currents and mechanically-evoked action potentials from all pulmonary NE cells (Fig. 2A, fig. S5B-D). About half of NE cells in the extrapulmonary bronchi were also mechanically sensitive, with the biophysical heterogeneity we observe (fig. S5D) possibly reflecting their transitional location between lung and trachea. In agreement with the electrophysiology recordings, we observed that mechanical stimulation drove calcium influx and that *Piezo2*[Cre] broadly labeled the pulmonary NE cells (Fig. 2B-D, fig. S5E). Moreover, we found that mechano-evoked currents were lost in *Piezo2*-null NE cells (cKO, *Ascl1*[CreERT2/+]; *Piezo2*[flox/flox]; *R26*[LSL-

tdTomato/+, Fig. 2E), thus conclusively demonstrating that *Piezo2* accounts for mechanical sensitivity in pulmonary NE cells.

In contrast to the lung, we found that the tracheal and laryngeal NE cells were largely unresponsive to mechanical stimuli, which we again assessed using electrophysiology, calcium imaging and histology (Fig. 2A-D, fig. S5B, C). Interestingly, published transcriptomic data of human tracheal and pulmonary NE cells (*39, 40*) support our observation that these specialized cells broadly express voltage-gated ion channels and synaptic release machinery and also exhibit differential expression of *Piezo2* (fig. S5F), highlighting generally conserved properties of NE cells in mammals.

Tracheal and laryngeal NE cells respond to aspiration-related stimuli
The function of tracheal and laryngeal NE cells in healthy airways is unknown. As the upper airway is the gateway to the lung, these regions are particularly sensitive to detecting noxious agents that could cause tissue damage and impair oxygen exchange. Water "going down the wrong pipe" and acid reflux are two commonly experienced examples of noxious stimuli that elicit protective airway reflexes (*8, 41–44*). Using calcium imaging in tissue slices from *Ascl1^{CreERT2}*; *Polr2a^{LSL-GCaMP5G, tdTomato}* mice, we found that these stimuli robustly activated tracheal and laryngeal NE cells (Fig. 3A-D).

We confirmed intrinsic sensitivity to acid using dissociated NE cells where stimuli below pH 4 promoted calcium influx (Fig. 3E, F). ASIC, TrpV1 or Otop channels are unlikely candidates for conferring pH sensitivity as their pH thresholds are too high (*45–47*) and none were detected in both our tracheal and laryngeal NE cell transcriptomes. Interestingly, however, acid responses were completely inhibited by a T-type calcium channel blocker (Fig. 3E), raising the possibility acidic solutions depolarize NE cells which then activates T-type Ca$_V$ channels.

We also found that dissociated tracheal and pulmonary NE cells were intrinsically sensitivity to water and exhibited calcium responses to osmolarities below 75 mOSM (Fig. 3G, fig. S6A), but only those in the lung required Piezo2 (fig. S6B), suggesting that tracheal NE cells utilize a distinct water-sensing mechanism. In tracheal NE cells, external calcium entry was required for water responses, but this likely does not involve Ca$_V$ channels since water application hyperpolarized the cells (fig. S6C, D). Therefore, we posit that water activates a non-Piezo2 cation channel in tracheal/laryngeal NE cells, such as *Tmem63a/b/c* (*48*).

Most importantly, our data show that tracheal and laryngeal NE cells are sensitive to two noxious stimuli, water and acid, that are known to provoke forceful airway clearance responses when inappropriately aspirated (*8, 49, 50*). We therefore sought to test the possibility that tracheal and laryngeal NE cells contribute to critical reflexes that protect the airway.

Tracheal and laryngeal NE cells communicate with neurons via purinergic signaling
Neurons expressing P2rx2/3 purinergic receptors densely innervate the trachea and larynx and reside in close proximity to tracheal NE cells (*51*). Furthermore, immortalized human small cell lung cancer lines have been shown to release ATP into the culture medium (*27*). To determine if NE cell stimulation evokes time-locked ATP release, we positioned a sniffer cell expressing the ATP1.0 biosensor (*52*) next to a dissociated NE cell. Indeed, we saw a robust change in biosensor fluorescence only upon stimulation of tracheal and laryngeal NE cells with super-threshold (-10 mV) voltage pulses or high potassium (Fig. 4A, B, fig. S7A-C). Responses were also elicited by

water, further validating its physiological relevance (fig. S7D). This is likely a vesicle-mediated processes since addition of calcium-free external saline, but not a Pannexin-1 inhibitor (^{10}panx)(53), blocked ATP release (Fig. 4C).

We next tested whether NE cells communicate with either the trachea/larynx-innervating recurrent laryngeal nerve (RLN) or the larynx-innervating superior laryngeal nerve (SLN). Using *ex vivo* whole-nerve recordings, we found that optogenetically activating NE cells (*Ascl1^{CreERT2}* crossed to *Rosa26$^{LSL-ReaChr}$* or *Rosa26$^{LSL-ChR2}$*) increased the rate of compound action potentials (CAP) in the SLN and RLN (Fig. 4D-F, fig. S8A-D). Consistent with known innervation patterns, activation of tracheal NE cells drove activity only in the RLN whereas activation of laryngeal NE cells drove activity in both fibers (Fig. 4E, F). Of note, *Ascl1^{CreERT2}* is not expressed in vagal neurons (fig. S8A). We did not observe a change in CAP rate when stimulating areas of the dish proximal to the nerve fiber or when using control ReaChR/ChR-only mice (Fig. 4E, F, fig. S8B), but application of high salt activated nerve fibers from experimental and control animals equivalently (fig. S8C, D).

To determine if stimulus-evoked ATP release from NE cells activates nearby P2x+ nerve fibers, we optogenetically stimulated NE cells and measured changes in light-evoked RLN or SLN activity in the presence of the broad, persistent P2x receptor antagonist, PPADS. Indeed, incubation with PPADS, but not vehicle, led to a significant reduction in firing rate evoked by NE cell stimulation, but not high salt (Fig. 4G, H, fig. S8E, F). Together, these data show that ATP release from laryngeal or tracheal NE cells activates airway-innervating nerve fibers.

Tracheal and laryngeal NE cells drive protective behavioral reflexes
The RLN and SLN drive protective behavioral reflexes such as laryngeal closure, cough, apnea, and swallowing when foreign substances like water or gastric acid enter the upper airway (8, 42, 43, 54). To test whether NE cell activation could initiate these defensive reflexes, we surgically exposed the airway of mice expressing ChR2 in NE cells (*Ascl1^{CreERT2}*; *Rosa26$^{LSL-ChR2}$*) and measured light-evoked changes in respiration (Fig. 5A). We found that optogenetic activation of airway NE cells primarily drove swallowing reflexes, which we identified as an apnea, or pause in breathing, that co-occurred with movement of the hyoid bone and electromyography (EMG) activity in the submental complex muscles (Fig. 5B-F). We also observed post-swallow expiratory reflexes, which is a protective reflex observed in humans to prevent aspiration (55, 56), and cough-like reflexes, which we define as a large exhalation preceded by a large inhalation (Fig. 5E, fig. S9A-C) (57).

Optogenetic activation of NE cells in the larynx, upper trachea and middle trachea consistently drove airway protective reflexes (Fig. 5F, fig. S9D, E, Movie S2-3). Reflexes were rarely observed in between light pulses, when the light was off-target, or in control ChR2-only animals (Fig. 5F). Of note, *Ascl1^{CreERT2}* labels a small subset of taste cells in laryngeal taste buds at the esophagus/airway junction (~2-3 cells/taste bud, fig. S10A). While optogenetic stimulation of all taste cells (*Krt8-CreER^{T2}; lsl-ChR2*) also drives airway protective reflexes (8), we do not observe off-target activation of taste cells when light is directed at the trachea (fig. S10B). Moreover, surgical ablation of the tissue containing the taste cells did not affect light-evoked nerve fiber activity in the SLN when optogenetically stimulating the NE cells (fig. S10C, D), which is consistent with their stark numerical difference (~50 taste cells vs >1000 laryngeal NE cells). Thus, we conclude that the primary driver of the light-evoked airway protective reflexes seen in our experimental paradigm results from activation of NE cells. Interestingly, since we observed

swallowing and cough at each stimulus location (fig. S9D), NE cells in the trachea and larynx likely feed into functionally similar downstream circuitry to drive both reflexes.

To test whether NE cells are necessary for protective reflexes, we adapted a preparation (*8*) where perfusion of water, acid, or high-salt over the larynx and upper trachea evoke robust swallowing reflexes (Fig. 5G). We used two orthologous diphtheria toxin-based methods to genetically ablate NE cells and the putatively acid-sensitive Type III laryngeal taste cells: $Ascl1^{CreERT2}$; $Rosa26^{lsl-Diphtheria\ Toxin\ A}$ (*lsl-DTA*) and $Ascl1^{CreERT2}$; $Rosa26^{lsl-Diphtheria\ Toxin\ A\ Receptor}$ (*lsl-DTR*) mice (fig S10E). With both genetic strategies, we found that water and acid elicited significantly fewer swallows following NE cell ablation compared to littermate control mice (Fig. 5H, fig. S10E, F). In contrast, there was no significant difference in the number of high salt- or mechanically-evoked swallows (Fig. 5H, fig. S10F). Thus, NE cells contribute to initiating protective behavioral reflexes in response to water or acid.

Discussion
The larynx is densely innervated by sensory neurons that drive protective reflexes like swallowing, apnea, and cough when noxious stimuli are aspirated into the airways (*8*, *42*, *43*, *54*). Elegant recent work has shown that activation of P2x2/P2x3 purinergic receptors on vagal sensory afferents drives water- and acid-evoked swallowing reflexes (*8*). By analogy to other sensory systems, it has been suggested that these neurons act as 'second order responders' downstream of specialized sensory cells that directly detect relevant physiologic stimuli (*58*). We now show that airway NE cells fulfill this role as they are sensitive to relevant stimuli and functionally couple with purinoceptive vagal afferents to elicit protective reflexes. Consistent with this proposed guardianship of the airways, we found that NE cells are substantially more abundant in the larynx than in extrapulmonary bronchi, matching the relative density of sensory nerve fibers in these locales. Interestingly, optogenetic activation of the laryngeal taste cells, which are located in the uppermost part of the airway, drives an expiratory reflex (large exhalation without a preceding inhalation) to prevent substances from entering the airway (*8*). In contrast, we show that NE cell activation drives a cough-like reflex (large exhalation preceded by a large inhalation) which is effective at expelling substances that have entered the airway. Ultimately, we propose that NE cells collaborate with laryngeal taste cells to provide layers of protection that prevent noxious stimuli from reaching the lungs.

Recent transcriptome profiling and histological studies suggest that NE cells are molecularly diverse (*22*, *30*). We now validate this idea at a functional level with several interesting observations. First, we demonstrate that pulmonary NE cells are mechanosensitive, whereas those in the larynx and trachea are not. This striking difference likely reflects the relative elasticity of the lung versus more rigid cartilaginous structures of the upper airway and the need to assess moment-to-moment volume changes in the latter. Furthermore, hypoxia has been proposed to increase excitability of pulmonary NE cells through inhibition of potassium channels (*23*, *59*), raising the possibility that environmental stimuli or other pathological states, like fibrosis, could enhance mechanical sensitivity. The other notable difference between pulmonary and upper airway NE cells is their capacity to fire single versus multiple action potentials, respectively. The functional relevance of this distinction is not yet clear, but may be related to the amount or type of transmitter released in response to a given stimulus. Indeed, NE cells are known to contain dense and light core vesicles for release of both peptides and small neurotransmitters (*12*, *60*). How biophysical differences among NE cell subpopulations relate to their stimulus sensitivities, signal transduction mechanisms, or relative release of distinct transmitter pools remain to be determined.

Moreover, in the one other demonstration of NE cell excitability, current injection into pulmonary NE cells from rabbits was shown to elicit multiple action potentials (*23*), suggesting that electrophysiological properties may also relate to species-specific physiological needs.

Previous studies have ascribed chronic, humoral functions to molecules released from NE cells (*15–18, 61*), but it has long been speculated that they communicate directly with nerve fibers to elicit acute physiologic or behavioral responses (*12, 62–64*). Our work now demonstrates this directly, and while we focus on purinergic signaling, serotonin likely mediates important physiologic actions as well since NE cells in the lung and specific parts of the larynx are serotonergic and reside in close apposition to neurons expressing 5-HT$_3$ receptors. Thus, deciphering the full range of physiological consequences of neurotransmitter release from NE cells remains an important, but still unexplored area of inquiry.

Dysphagia and aspiration into the lungs account for morbidity and mortality across a range of age groups and clinical settings, but especially for the elderly and/or those afflicted with disorders that compromise motor function (e.g., stroke or neurodegenerative diseases) (*1–4*). Both basic and clinical studies suggest that sensory pathways must be considered as important control points and therapeutic targets for regulating swallowing, cough, and other airway protective reflexes (*58, 65–68*). Indeed, a P2x3 receptor antagonist (gefapixant) has recently been shown to reduce coughing frequency in patients suffering from refractory chronic cough (*69*). Our work now raises the possibility that functional interactions between NE cells and purinoceptive sensory afferents contribute to disease symptoms. Thus, our detailed characterization of molecular mechanisms underlying NE cell activation may reveal additional therapeutic strategies for treating disorders of cough or other aspects of airway protection and hyper-reactivity.
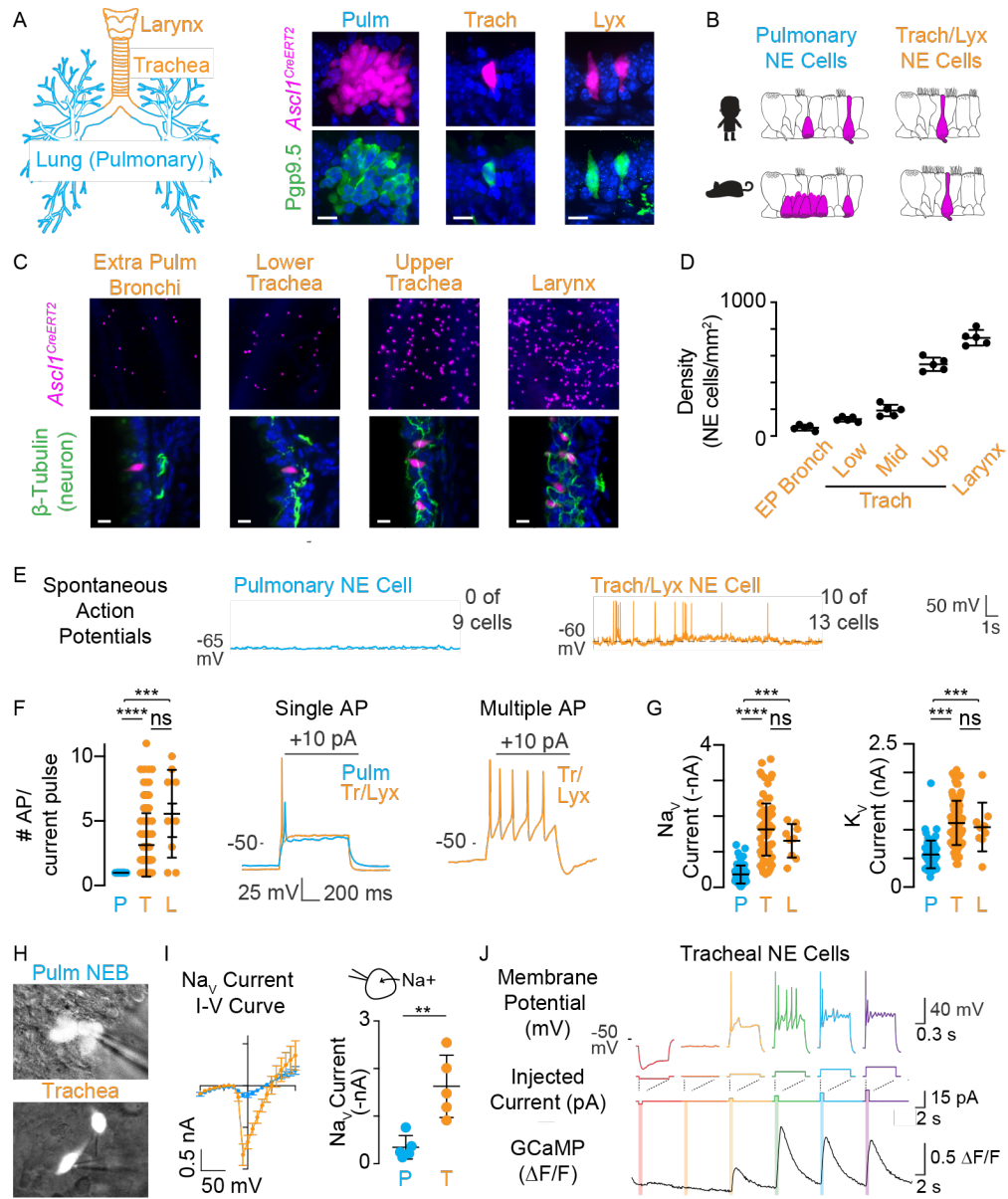
Fig. 1.

A

Larynx
Trachea
Lung (Pulmonary)

Pulm | Trach | Lyx

Ascl1^CreERT2

Pgp9.5

B

Pulmonary NE Cells | Trach/Lyx NE Cells

C

Extra Pulm Bronchi | Lower Trachea | Upper Trachea | Larynx

Ascl1^CreERT2

β-Tubulin (neuron)

D

Density (NE cells/mm²)

1000

EP Bronch   Low Mid   Up   Larynx
                 Trach

E

Spontaneous Action Potentials

Pulmonary NE Cell   0 of 9 cells
-65 mV

Trach/Lyx NE Cell   10 of 13 cells
-60 mV

50 mV | 1s

F

**** ***
ns

AP/current pulse

10

5

P T L

Single AP
+10 pA

Pulm
Tr/Lyx
-50

Multiple AP
+10 pA

Tr/Lyx
-50

25 mV | 200 ms

G

**** ***
ns

Na_V Current (-nA)

4

P T L

*** ***
ns

K_V Current (nA)

2.5

P T L

H

Pulm NEB

Trachea

I

Na_V Current I-V Curve

0.5 nA
50 mV

Na+

**

Na_V Current (-nA)

3

P T

J

Tracheal NE Cells

Membrane Potential (mV)
-50 mV

40 mV
0.3 s

Injected Current (pA)

15 pA
2 s

GCaMP (ΔF/F)

0.5 ΔF/F
2 s

Fig. 1. Morphological and biophysical diversity of neuroendocrine cells across the airway.
(**A**) Diagram of the airway (left). Co-localization of $Ascl1^{CreERT2}$; $R26^{lsl\text{-}TdTomato}$ (pink), a neuroendocrine marker Pgp9.5 (green) and DAPI nuclear stain (blue) in lung (left, middle), trachea (right, middle) and larynx (right). Representative images from $n = 5$ mice. (**B**) Cartoon of NE cell morphology (pink) in mouse and human airway epithelium. (**C**) Whole mount (top) and slice (bottom) histology of NE cells (pink) with neurons marked by β-Tubulin (green, bottom) and DAPI (blue). Representative images from $n = 5$ mice. (**D**) Density of NE cells in extra pulmonary bronchi (EP Bronch), trachea (Trach) and larynx, $n = 5$ mice. (**E**) Spontaneous action potentials recorded at resting membrane potential in dissociated cells, $n = 9\text{-}13$ cells. (**F, G**) Biophysical characteristics of dissociated pulmonary (P, $n = 68$ cells), tracheal (T, $n = 99$ cells) and laryngeal (L, $n = 9$ cells) NE cells. All data were analyzed with Kruskal-Wallis ($P{<}0.0001$) and Dunn's multiple comparisons test. (**F**) Number of action potentials elicited by depolarizing current injection (left) for pulmonary (P, blue) or tracheal/laryngeal (T/L, orange) NE cells together with representative traces (middle and right). (**G**) Peak inward voltage-gated currents (Na_V, left) and steady-state outward currents at 30 mV (K_V, right). (**H, I**) Slice electrophysiology recordings. Representative images (**H**) and current-voltage trace (**I**, left). Peak inward voltage-gated currents (**I**, right) for pulmonary (P) and tracheal (T) NE cells, $n = 5$ cells. Unpaired t test, $P = 0.0035$. (**J**) Representative tracheal NE patch-clamp-imaging trace. Current (middle) was injected into NE cell while recording membrane potential (top) and change in GCaMP fluorescence (bottom). Image scale bars 10 μm. * $P < 0.05$, ** $P < 0.01$, *** $P < 0.001$ and **** $P < 0.0001$. Data represented as mean +/- SD. See Table S1 for extended detail on statistics and P-values.
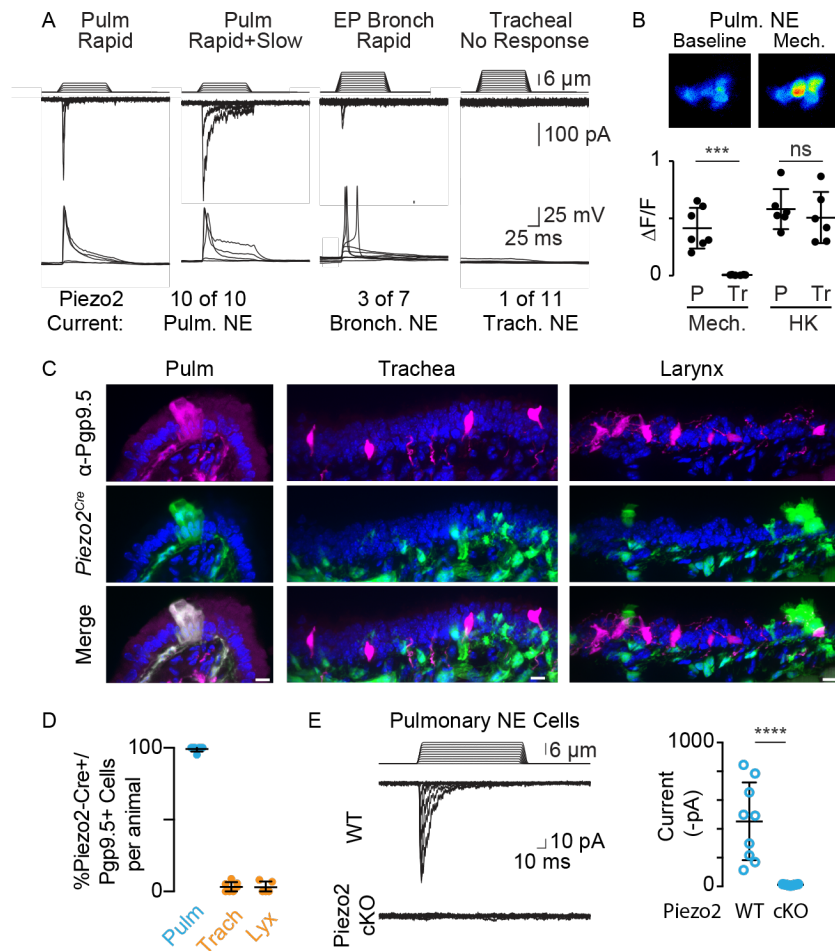
Fig. 2.

Fig. 2. Airway NE cells are differentially mechanosensitive. (**A**) Representative patch-clamp recordings of mechanically-evoked currents (middle) and action potentials (bottom) aligned to displacement of mechanical probe (top) showing number and type of mechanosensitive cells, including pulmonary or extra pulmonary (EP) bronchial NE cells with slowly and/or rapidly inactivating currents, and mechanically insensitive tracheal NE cells. (**B**) Representative image showing GCaMP response by a pulmonary NE cell cluster to mechanical stimulation (top). Quantification of calcium response to mechanical stimulation (mech) or high potassium (HK) in explant preparations (bottom). $n = 6$-7 cells. Unpaired t-test with Welch's correction (mechanical, $P = 0.0009$ and HK, $P = 0.5444$). (**C, D**) Representative images (**C**) and quantification (**D**) of co-localization of $Piezo2^{Cre}$; $R26^{lsl\text{-}TdTomato}$ (green), the NE cell marker Pgp9.5 (pink) and DAPI nuclear stain (blue) across the airways. $n = 5$-7 mice. (**E**) Representative traces (left) and quantification (right) of mechanical activation of pulmonary NE cells from WT mice or mice with conditional deletion of $Piezo2$ (cKO). $n = 9$ cells, Mann-Whitney test, $P < 0.0001$. Image scale bars 10 μm. * $P < 0.05$, ** $P < 0.01$, *** $P < 0.001$ and **** $P < 0.0001$. Data represented as mean +/- SD. See Table S1 for extended detail on statistics and P-values.
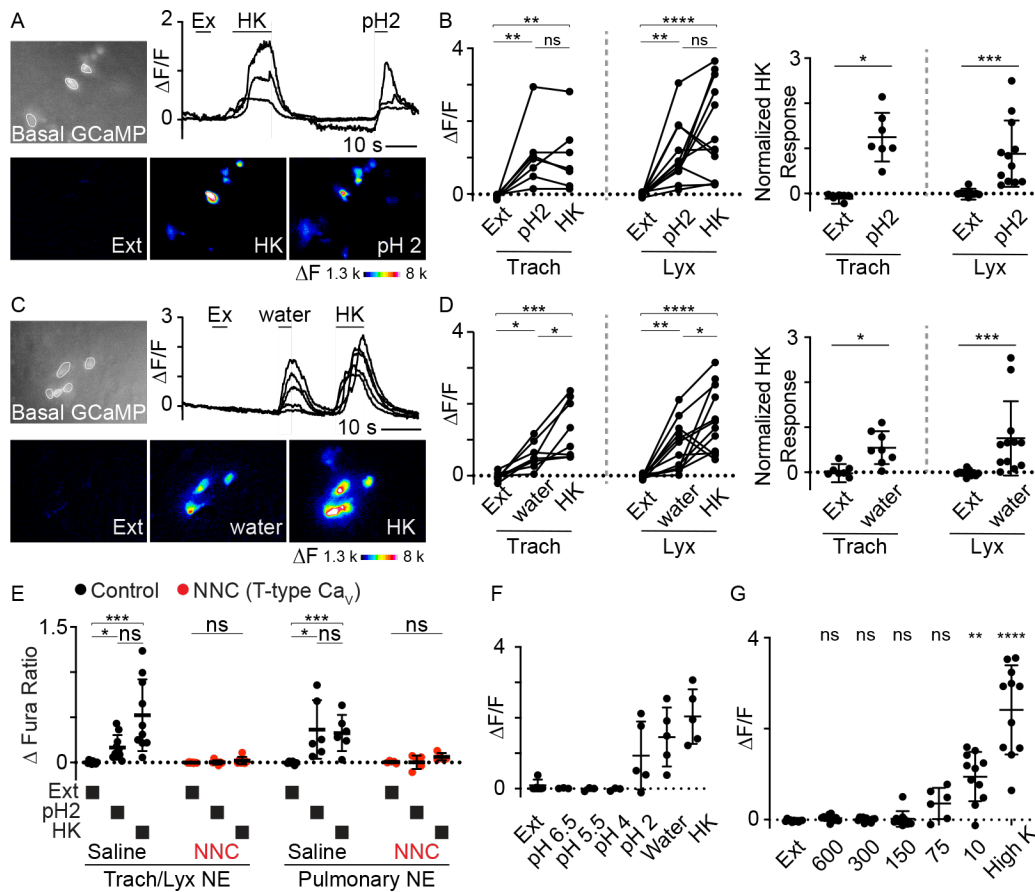
Fig. 3.

Fig. 3. Airway NE cells respond to acid and water. (**A**-**D**) Calcium imaging of NE cells in tracheal (trach) and laryngeal (lyx) tissue in response to low pH (**A**, **B**) or water (**C**, **D**) versus high potassium (HK). White circles in images mark cells analyzed for representative traces. Rainbow scale indicates change in fluorescence. Quantification of responses (**B**, **D**, left). Repeated measures one-way ANOVA (B, Trach $P < 0.0038$, B, Lyx $P <0.0001$, D, Trach $P = 0.0002$ and D, Lyx $P < 0.0001$) and Tukey's multiple comparisons test for each tissue/stimulus pair. Calcium responses normalized to HK response (**B**, **D**, right). Wilcoxon signed rank test for trach pH 2, lyx pH 2, trach water and lyx water, respectively: $n = 7$, 12, 8 and 12 cells and $P = 0.0156$, 0.0005, 0.0156, and 0.0005. (**E**) Quantification of calcium responses in dissociated cells in the absence (black) or presence (red) of the T-type calcium channel blocker NNC 55-0396 adjusted for baseline Fura-2 ratio (delta Fura Ratio). Responses are to external saline (ext), pH2 or HK. Friedman test for Trach/Lyx Saline, NNC, Pulmonary Saline, NNC, respectively: ($P < 0.0001$, $P = 0.96$, $P =0.0081$ and $P = 0.093$, respectively) and Dunn's multiple comparisons test. (**F**, **G**) Calcium responses to a range of acidities (**F**) or osmolarities (**G**). Kruskal-Wallis test ($P < 0.0001$) with Dunn's multiple comparisons test to external saline. * $P < 0.05$, ** $P < 0.01$, *** $P < 0.001$ and **** $P < 0.0001$. Data represented as mean +/- SD. See Table S1 for extended detail on statistics and P-values.

Fig. 4.

A

ATP Sensor

0.2 ΔF/F

5s

NE Cell

Pulse −70 mV

Pulse −10 mV

ATP1.0

NE

B

ΔF/F

mV: −70 −10   −70 −10

Trach   Larynx

** ***

C

Block ATP Release via:

Panx1   Vesicles

** ns

ΔF/F

mV: −70 −10   −70 −10

^{10}Panx   No Ext. Ca^{2+}

D

Off Lyx

On Lyx   SLN

On Trach   RLN

Off Trach   Ex vivo Recording Electrode

E   SLN - Superior Laryngeal Nerve

On Lyx

0.1 µV   20 s

CAP/min

Opto: − +   − +   − +

On Lyx   On Trach   Off Lyx

* ns ns

Ascl1^{CreERT2}; Isl-ReaChR

F   RLN - Recurrent Laryngeal Nerve

On Trach

20 s

CAP/min

Opto: − +   − +   − +

On Lyx   On Trach   Off Trach

* * ns

Ascl1^{CreERT2}; Isl-ReaChR

G   Ex vivo Recording: Superior Laryngeal Nerve
Ascl1^{CreERT2}; Isl-ChR2

P2x Receptor Inhibition   Control

20 s

0.1 s

Pre-PPADs   Post-PPADs   Pre-Saline   Post-Saline

H

Fraction of # CAPs (Post/Pre)

Saline   +   +
PPADs   +   +
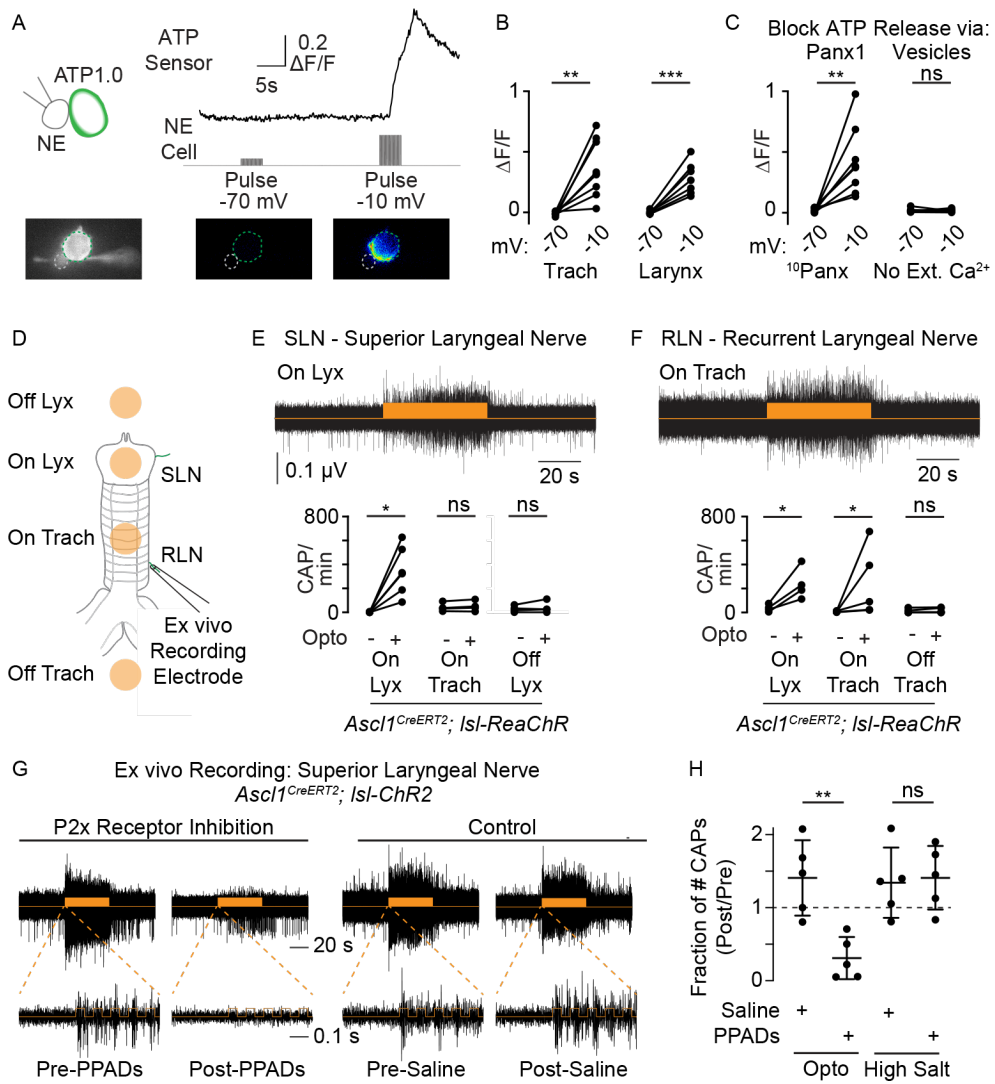
Opto   High Salt

** ns

Fig. 4. Upper airway NE cells release ATP and activate purinoceptive neurons. (**A**) Schematic of NE cell adjacent to an ATP biosensor cell (ATP1.0-expressing HEK293T cell). Representative trace (top) and images (bottom) of biosensor cell responses when NE cell is pulsed to -70 mV or -10 mV. (**B**, **C**) Quantification of changes in biosensor fluorescence in (**B**) tracheal or laryngeal NE cells or (**C**) tracheal NE cells incubated with [10]Panx or calcium-free external saline. **B**: n = 7-9 cells, paired t-test, P = 0.0015 and 0.0009, respectively. **C**: n = 7-8 cells, paired t-test, P = 0.0061 and 0.805, respectively. (**D**) Schematic of *ex vivo* whole nerve electrophysiology preparation for recording superior laryngeal nerve (SLN) or recurrent laryngeal nerve (RLN) activity in response to optogenetic activation (orange dots). (**E**, **F**) Representative trace of spiking activity (black) in SLN (**E**) or RLN (**F**) in response to optogenetic activation (orange bar) (top). Number of compound action potentials (CAP) in the minute before (-) or during (+) optogenetic stimulation of larynx, trachea, or area adjacent to the preparation (off) in *Ascl1*^{CreERT2}; *R26*$^{lsl-ReaChR}$ animals (bottom). **E**: Wilcoxon signed rank test, n = 4-6 preparations (P = 0.0312, 0.25, 0.875, respectively). **F**: n = 4-7 preparations, paired t test (P = 0.0355, 0.0233, 0.7663, respectively). (**G**) Effect of P2x receptor antagonist (PPADS, representative trace, left) or vehicle (representative trace, right) on light-evoked activity in SLN. (**H**) Quantification of suppression of SLN activity (# post CAPS/# pre CAPS) for optogenetic or high salt activation with PPADS or vehicle control, n = 5 preparations. Unpaired t-test, P = 0.0032 and = 08232, respectively. * P < 0.05, ** P < 0.01, and *** P < 0.001. Data represented as mean +/- SD. See Table S1 for extended detail on statistics and P-values.
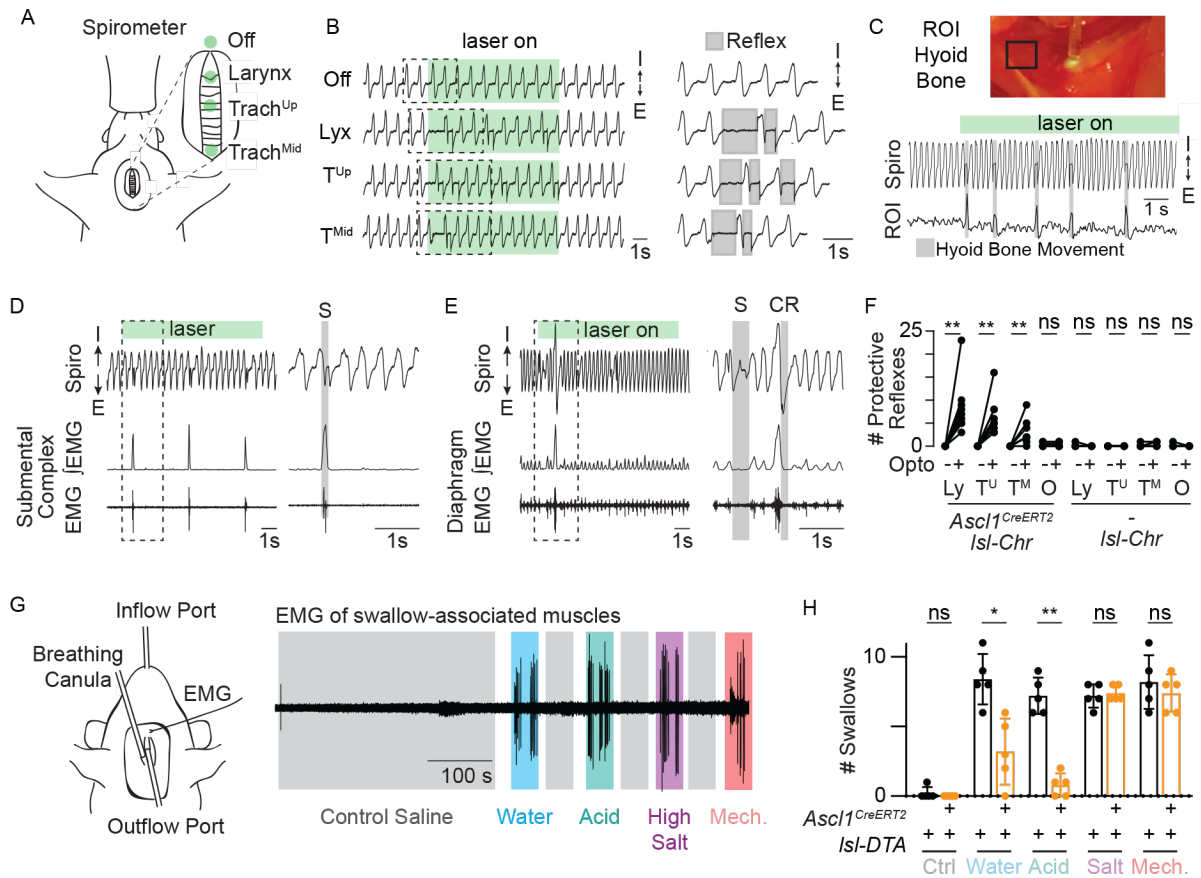
Fig. 5.

Fig. 5. Upper airway NE cells drive protective behavioral responses. (**A**) Schematic of whole animal preparation with green dots representing approximate location of optogenetic stimulation. (**B**) Airway protective reflexes following optogenetic stimulation of NE cells. Representative spirometry traces during optogenetic stimulation (green, laser on) of NE cells ($Ascl1^{CreERT2}$; $R26^{lsl-ChR2}$) in the larynx (lyx), upper trachea (T^{Up}), mid-trachea (T^{Mid}) and outside of airway. I = inspiration, E = expiration. (**C**) Representative image of hyoid bone ROI (top). Spirometry traces illustrating alignment of apneas with deflections in the hyoid bone. (**D**, **E**) Spirometry traces (top) aligned to electromyography (EMG) recordings of submental complex during representative swallow (**D**) or diaphragm during representative cough-like reflex and swallow (**E**). Integrated (middle) and raw (bottom) EMG traces depicted. (**F**) Quantification of # of protective reflexes (swallowing or cough-like reflex) before (-) and during (+) 3x 10 s stimulation bouts. Larynx (Ly), upper trachea (T^{U}), mid-trachea (T^{M}) and off airway (O) for $Ascl1^{CreERT2}$; $R26^{lsl-ChR}$ and $R26^{lsl-ChR}$ animals (n = 5-7 animals). Wilcoxon signed rank test (P = 0.0156, 0.0156, 0.0156, >0.99, >0.99, >0.99, 0.5, >0.99, * P < 0.05. (**G**) Schematic (left) and representative EMG trace (right) of airway perfusion assay. (**H**) Quantification of stimulus-evoked swallows with and without NE cell ablation. Mann Whitney Test comparing responses in Cre+ vs Cre- for each stimulus (n = 5, P > 0.999, = 0.0159, = 0.0079, > 0.9999, = 0.6429). EMG, movement analysis and spirometry traces are arbitrary units. Data represented as mean +/- SD. See Table S1 for extended detail on statistics and P-values.

References

1. T. Pitts, M. J. Rose, A. N. Mortensen, I. Poliacek, C. M. Sapienza, B. G. Lindsey, K. F. Morris, P. W. Davenport, D. C. Bolser, Coordination of cough and swallow: A meta-behavioral response to aspiration. *Respir. Physiol. Neurobiol.* **189**, 543–551 (2013).

2. C. A. S. Hammond, L. B. Goldstein, R. D. Horner, J. Ying, L. Gray, L. Gonzalez-Rothi, D. C. Bolser, Predicting aspiration in patients with ischemic stroke. *Chest*. **135**, 769–777 (2009).

3. S. K. Daniels, K. Brailey, D. H. Priestly, L. R. Herrington, L. A. Weisberg, A. L. Foundas, Aspiration in patients with acute stroke. *Arch Phys Med Rehabil*. **79**, 14–19 (1998).

4. D. L. Doggett, K. A. Tappe, M. D. Mitchell, R. Chapell, V. Coates, C. M. Turkelson, Prevention of pneumonia in elderly stroke patients by systematic diagnosis and treatment of dysphagia: An evidence-based comprehensive analysis of the literature. *Dysphagia*. **16**, 279–295 (2001).

5. L. Y. Lee, J. Yu, Sensory nerves in lung and airways. *Compr. Physiol.* **4**, 287–324 (2014).

6. S. B. Mazzone, B. J. Undem, Vagal afferent innervation of the airways in health and disease. *Physiol. Rev.* **96**, 975–1024 (2016).

7. S. H. Kim, M. J. Patil, S. H. Hadley, P. K. Bahia, S. G. Butler, M. Madaram, T. E. Taylor-Clark, Mapping of the sensory innervation of the mouse lung by specific vagal and dorsal root ganglion neuronal subsets. *eNeuro*. **9**, 1–41 (2022).

8. S. L. Prescott, B. D. Umans, E. K. Williams, R. D. Brust, S. D. Liberles, An airway protection program revealed by sweeping genetic control of vagal afferents. *Cell*. **181**, 574–589 (2020).

9. T. E. Finger, V. Danilova, J. Barrows, D. L. Bartel, A. J. Vigers, L. Stone, G. Hellekant, S. C. Kinnamon, Neuroscience: ATP signalling is crucial for communication from taste buds to gustatory nerves. *Science*. **310**, 1495–1499 (2005).

10. G. Krasteva, B. J. Canning, P. Hartmann, T. Z. Veres, T. Papadakis, C. Mühlfeld, K. Schliecker, Y. N. Tallini, A. Braun, H. Hackstein, N. Baal, E. Weihe, B. Schütz, M. Kotlikoff, I. Ibanez-Tallon, W. Kummer, Cholinergic chemosensory cells in the trachea regulate breathing. *Proc. Natl. Acad. Sci.* **108**, 9478–9483 (2011).

11. N. W. Bellono, J. R. Bayrer, D. B. Leitch, J. Castro, C. Zhang, T. A. O'Donnell, S. M. Brierley, H. A. Ingraham, D. Julius, Enterochromaffin cells are gut chemosensors that couple to sensory neural pathways. *Cell*. **170**, 185–198 (2017).

12. J. M. Lauweryns, M. Cokelaere, P. A. L. Theunynck, Serotonin producing neuroepithelial bodies in rabbit respiratory mucosa. *Science*. **180**, 410–413 (1973).

13. H. Song, E. Yao, C. Lin, R. Gacayan, M.-H. Chen, P.-T. Chuang, Functional characterization of pulmonary neuroendocrine cells in lung development, injury, and tumorigenesis. *Proc. Natl. Acad. Sci.* **109**, 17531–17536 (2012).

14. Y. Ouadah, E. R. Rojas, D. P. Riordan, S. Capostagno, C. S. Kuo, M. A. Krasnow, Rare Pulmonary Neuroendocrine Cells Are Stem Article Rare Pulmonary Neuroendocrine Cells Are Stem Cells Regulated by Rb , p53 , and Notch Regulated, Cells. *Cell*. **179**, 403–416 (2019).

15. M. Shivaraju, U. K. Chitta, R. M. H. Grange, I. H. Jain, D. Capen, L. Liao, J. Xu, F. Ichinose, W. M. Zapol, V. K. Mootha, J. Rajagopal, Airway stem cells sense hypoxia and differentiate into protective solitary neuroendocrine cells. *Science*. **371**, 52–57 (2021).

16. P. Sui, D. L. Wiesner, J. Xu, Y. Zhang, J. Lee, S. Van Dyken, A. Lashua, C. Yu, B. S. Klein, R. M. Locksley, G. Deutsch, X. Sun, Pulmonary neuroendocrine cells amplify allergic asthma responses. *Science*. **360**, 1–10 (2018).

17. J. Barrios, K. R. Patel, L. Aven, R. Achey, M. S. Minns, Y. Lee, V. E. Trinkaus-randall, X. Ai, Early life allergen-induced mucus overproduction requires augmented neural stimulation of pulmonary neuroendocrine cell secretion. *FASEB J.* **31**, 4117–4128 (2017).

18. K. Branchfield, L. Nantie, J. M. Verheyden, P. Sui, M. D. Wienhold, X. Sun, Pulmonary neuroendocrine cells function as airway sensors to control lung immune response. *Science*. **351**, 707–710 (2016).

19. Y. Lu, Y. Huang, J. Li, J. Huang, L. Zhang, J. Feng, J. Li, Q. Xia, Q. Zhao, L. Huang, S. Jiang, Eosinophil extracellular traps drive asthma progression through neuro-immune signals. *Nat. Cell Biol.* **23**, 1060–1072 (2021).

20. A. Ferlito, C. E. Silver, C. R. Bradford, A. Rinaldo, Neuroendocrine neooplasms of the larynx: an overview. *Head Neck*. **36**, 1634–1646 (2014).

21. C. Swanton, R. Govindan, Clinical Implications of Genomic Discoveries in Lung Cancer. *N. Engl. J. Med.*, 1864–1873 (2016).

22. C. S. Kuo, S. Darmanis, A. Diaz de Arce, Y. Liu, N. Almanzar, T. T. H. Wu, S. R. Quake, M. A. Krasnow, Neuroendocrinology of the lung revealed by single cell RNA sequencing. *Elife*, 1–32 (2022).

23. C. Youngson, C. Nurse, H. Yeger, E. Cutz, Oxygen sensing in airway chemoreceptors. *Nature*. **365**, 153–155 (1993).

24. J. Pan, I. Copland, M. Post, H. Yeger, E. Cutz, Mechanical stretch-induced serotonin release from pulmonary neuroendocrine cells: Implications for lung development. *Am. J. Physiol. - Lung Cell. Mol. Physiol.* **290**, 185–193 (2006).

25. X. W. Fu, C. A. Nurse, V. Wong, E. Cutz, Hypoxia-induced secretion of serotonin from intact pulmonary neuroepithelial bodies in neonatal rabbit. *J. Physiol.* **539**, 503–510 (2002).

26. X. Gu, P. H. Karp, S. L. Brody, R. A. Pierce, M. J. Welsh, M. J. Holtzman, Y. Ben-Shahar, Chemosensory functions for pulmonary neuroendocrine cells. *Am. J. Respir. Cell Mol. Biol.* **50**, 637–646 (2014).

27. W. Yu, T. O. Moninger, M. V. Rector, D. A. Stoltz, M. J. Welsh, Pulmonary neuroendocrine cells sense succinate to stimulate myoepithelial cell contraction. *Dev. Cell*. **57**, 2221–2236 (2022).

28. R. Lembrechts, I. Brouns, K. Schnorbusch, I. Pintelon, P. J. Kemp, J. P. Timmermans, D. Riccardi, D. Adriaensen, Functional expression of the multimodal extracellular calcium-sensing receptor in pulmonary neuroendocrine cells. *J. Cell Sci.* **126**, 4490–4501 (2013).

29. M. Borges, R. I. Linnoila, H. J. K. Van De Velde, H. Chen, B. D. Nelkin, M. Mabry, S. B. Baylin, D. W. Ball, An achaete-scute homologue essential for neuroendocrine

differentiation in the lung. *Nature*. **386**, 852–855 (1997).

30. H. Mou, Y. Yang, M. A. Riehs, J. Barrios, M. Shivaraju, A. L. Haber, D. T. Montoro, K. Gilmore, E. A. Haas, B. Paunovic, J. Rajagopal, S. O. Vargas, R. L. Haynes, A. Fine, W. V. Cardoso, X. Ai, Airway basal stem cells generate distinct subpopulations of PNECs. *Cell Rep.* **35**, 1–8 (2021).

31. J. R. Gosney, M. C. J. Sissons, R. O. Allibone, Neuroendocrine cell populations in normal human lungs: A quantitative study. *Thorax*. **43**, 878–882 (1988).

32. M. Weichselbaum, M. P. Sparrow, E. J. Hamilton, P. J. Thompson, D. A. Knight, A confocal microscopic study of solitary pulmonary neuroendocrine cells in human airway epithelium. *Respir. Res.* **6**, 1–11 (2005).

33. W. Mahmoud, A. Perniss, K. Poharkar, A. Soultanova, U. Pfeil, A. Hoek, S. Bhushan, T. Hain, U. Gärtner, W. Kummer, CXCL13 is expressed in a subpopulation of neuroendocrine cells in the murine trachea and lung. *Cell Tissue Res.* **390**, 35–49 (2022).

34. M. A. Navarro, A. Salari, J. L. Lin, L. M. Cowan, N. J. Penington, M. Milescu, L. S. Milescu, Sodium channels implement a molecular leaky integrator that detects action potentials and regulates neuronal firing. *Elife*. **9**, 1–24 (2020).

35. S. A. N. Goldstein, D. A. Bayliss, D. Kim, F. Lesage, L. D. Plant, Nomenclature and Molecular Relationships of Two-P Potassium Channels. *Pharmacol. Rev.* **57**, 527–540 (2005).

36. B. Katz, R. Miledi, Ionic requirements of synaptic transmitter release. *Nature*. **215**, 651 (1967).

37. K. Nonomura, S. Woo, R. B. Chang, A. Gillich, Z. Qiu, A. G. Francisco, S. S. Ranade, S. D. Liberles, A. Patapoutian, C. Neuroscience, D. Neuroscience, L. Jolla, S. Diego, Piezo2 senses airway stretch and mediates lung inflationinduced apnoea. *Nature*. **541**, 176–181 (2017).

38. R. Lembrechts, I. Brouns, K. Schnorbusch, I. Pintelon, J. P. Timmermans, D. Adriaensen, Neuroepithelial bodies as mechanotransducers in the intrapulmonary airway epithelium: Involvement of TRPC5. *Am. J. Respir. Cell Mol. Biol.* **47**, 315–323 (2012).

39. K. J. Travaglini, A. N. Nabhan, L. Penland, R. Sinha, A. Gillich, R. V. Sit, S. Chang, S. D. Conley, Y. Mori, J. Seita, G. J. Berry, J. B. Shrager, R. J. Metzger, C. S. Kuo, N. Neff, I. L. Weissman, S. R. Quake, M. A. Krasnow, A molecular cell atlas of the human lung from single-cell RNA sequencing. *Nature*. **587**, 619–625 (2020).

40. K. C. Goldfarbmuren, N. D. Jackson, S. P. Sajuthi, N. Dyjack, K. S. Li, C. L. Rios, E. G. Plender, M. T. Montgomery, J. L. Everman, P. E. Bratcher, E. K. Vladar, M. A. Seibold, Dissecting the cellular specificity of smoking effects and reconstructing lineages in the human airway epithelium. *Nat. Commun.* **11** (2020), doi:10.1038/s41467-020-16239-z.

41. M. Szereda-Przestaszewska, J. G. Widdicombe., Reflex changes in the lumen of the cat larynx due to chemical irritation of the upper airways. *J. Physiol.* **232**, 80–81 (1973).

42. T. Shingai, Y. Miyaoka, R. Ikarashi, K. Shimada, Swallowing reflex elicited by water and taste solutions in humans. *Am. J. Physiol. Integr. Comp. Physiol.* **256**, 822–826 (1989).

43. H. W. Sundell, Laryngeal Chemoreflex in Newborn Lambs : *Pediatr. Res.* **13**, 1144–1149

(1979).

44. A. H. Morice, G. A. Fontana, M. G. Belvisi, S. S. Birring, K. F. Chung, P. V. Dicpinigaitis, J. A. Kastelik, L. P. McGarvey, J. A. Smith, M. Tatar, J. Widdicombe, ERS guidelines on the assessment of cough. *Eur. Respir. J.* **29**, 1256–1276 (2007).

45. S. E. Jordt, M. Tominaga, D. Julius, Acid potentiation of the capsaicin receptor determined by a key extracellular site. *Proc. Natl. Acad. Sci. U. S. A.* **97**, 8134–8139 (2000).

46. S. Kellenberger, L. Schild, International union of basic and clinical pharmacology. XCI. structure, function, and pharmacology of acid-sensing ion channels and the epithelial Na+ channel. *Pharmacol. Rev.* **67**, 1–35 (2015).

47. B. Teng, J. P. Kaplan, Z. Liang, Z. Krieger, Y. H. Tu, B. Burendei, A. B. Ward, E. R. Liman, Structural motifs for subtype-specific pH-sensitive gating of vertebrate otopetrin proton channels. *Elife*. **11**, 1–19 (2022).

48. H. Du, C. Ye, D. Wu, Y. Y. Zang, L. Zhang, C. Chen, X. Y. He, J. J. Yang, P. Hu, Z. Xu, G. Wan, Y. S. Shi, The cation channel TMEM63B is an osmosensor required for hearing. *Cell Rep.* **31**, 1–14 (2020).

49. B. R. Harding, P. Johnson, M. E. Mcclelland, Liquid-sensitive laryngeal receptors in the developing sheep, cat and monkey. *J. Physiol.* **277**, 409–422 (1978).

50. G. Sant'Ambrogio, J. W. Anderson, F. B. Sant'Ambrogio, O. P. Mathew, Response of laryngeal receptors to water solutions of different osmolality and ionic composition. *Respir. Med.* **85**, 57–60 (1991).

51. N. Takahashi, N. Nakamuta, Y. Yamamoto, Morphology of P2X3-immunoreactive nerve endings in the rat laryngeal mucosa. *Histochem. Cell Biol.* **145**, 131–146 (2016).

52. Z. Wu, K. He, Y. Chen, H. Li, S. Pan, B. Li, T. Liu, F. Xi, F. Deng, H. Wang, J. Du, M. Jing, Y. Li, A sensitive GRAB sensor for detecting extracellular ATP in vitro and in vivo. *Neuron*. **110**, 770–782 (2022).

53. R. J. Thompson, M. F. Jackson, M. E. Olah, R. L. Rungta, D. J. Hines, M. A. Beazely, J. F. MacDonald, B. A. MacVicar, Activation of pannexin-1 hemichannels augments aberrant bursting in the hippocampus. *Science*. **322**, 1555–1559 (2008).

54. T. Y. Shen, M. C. Pertzborn, M. J. Rose, M. N. Musselwhite, P. W. Davenport, D. C. Bolser, Influence of intrathoracic vagotomy on the cough reflex in the anesthetized cat. *Respir. Physiol. Neurobiol.* **296**, 1–7 (2022).

55. A. Huff, M. D. Reed, B. K. Smith, E. H. Brown, A. V. Ovechkin, T. Pitts, Strategies for the integration of cough and swallow to maintain airway protection in humans. *Lung*. **196**, 601–608 (2018).

56. J. G. Widdicombe, W. R. Addington, G. A. Fontana, R. E. Stephens, Voluntary and reflex cough and the expiration reflex; implications for aspiration after stroke. *Pulm. Pharmacol. Ther.* **24**, 312–317 (2011).

57. C. L. Ludlow, Laryngeal Reflexes: Physiology, Technique, and Clinical Use. *J. Clin. Neurophysiol.* **32**, 284–293 (2015).

58. Y. Moayedi, M. J. Pitman, J. C. de Nooij, Airway protection— a role for vagal P2RY1

receptors. *Cell*. **181**, 509–511 (2020).

59. X. W. Fu, D. Wang, C. A. Nurse, M. C. Dinauer, E. Cutz, NADPH oxidase is an O2 sensor in airway chemoreceptors: Evidence from K+ current modulation in wild-type and oxidase-deficient mice. *Proc. Natl. Acad. Sci.* **97**, 4374–4379 (2000).

60. R. I. Linnoila, Functional facets of the pulmonary neuroendocrine system. *Lab. Investig.* **86**, 425–444 (2006).

61. J. Xu, L. Xu, P. Sui, J. Chen, E. A. Moya, P. Hume, W. J. Janssen, J. M. Duran, P. Thistlethwaite, A. Carlin, P. Gulleman, B. Banaschewski, M. K. Goldy, J. X. J. Yuan, A. Malhotra, G. Pryhuber, L. Crotty-Alexander, G. Deutsch, L. R. Young, X. Sun, Excess neuropeptides in lung signal through endothelial cells to impair gas exchange. *Dev. Cell*. **57**, 839–853 (2022).

62. J. Xu, H. Yu, X. Sun, Less Is More: Rare Pulmonary Neuroendocrine Cells Function as Critical Sensors in Lung. *Dev. Cell*. **55**, 123–132 (2020).

63. E. Cutz, J. Pan, H. Yeger, N. J. Domnik, J. T. Fisher, Recent advances and controversies on the role of pulmonary neuroepithelial bodies as airway sensors. *Semin. Cell Dev. Biol.* **24**, 40–50 (2013).

64. S. L. Prescott, S. D. Liberles, Internal senses of the vagus nerve. *Neuron*. **110**, 579–599 (2022).

65. M. Z. Hossain, H. Ando, S. Unno, J. Kitagawa, Targeting chemosensory ion channels in peripheral swallowing-related regions for the management of oropharyngeal dysphagia. *Int. J. Mol. Sci.* **21**, 1–45 (2020).

66. K. F. Chung, *Pharmacology and therapeutics of cough: Clinical cough VI: The need for new therapies for cough: disease-specific and symptom-related antitussives* (1978), vol. 54.

67. S. B. Mazzone, L. McGarvey, Mechanisms and rationale for targeted therapies in refractory and unexplained chronic cough. *Clin. Pharmacol. Ther.* **109**, 619–636 (2021).

68. L. Rofes, V. Arreola, A. Martin, P. Clavé, Natural capsaicinoids improve swallow response in older patients with oropharyngeal dysphagia. *Gut*. **62**, 1280–1287 (2013).

69. L. P. McGarvey, S. S. Birring, A. H. Morice, P. V. Dicpinigaitis, I. D. Pavord, J. Schelfhout, A. M. Nguyen, Q. Li, A. Tzontcheva, B. Iskold, S. A. Green, C. La Rosa, D. R. Muccino, J. A. Smith, Efficacy and safety of gefapixant, a P2X3 receptor antagonist, in refractory chronic cough and unexplained chronic cough (COUGH-1 and COUGH-2): results from two double-blind, randomised, parallel-group, placebo-controlled, phase 3 trials. *Lancet*. **399**, 909–923 (2022).

70. J. Battiste, A. W. Helms, E. J. Kim, T. K. Savage, D. C. Lagace, C. D. Mandyam, A. J. Eisch, G. Miyoshi, J. E. Johnson, Ascl 1 defines sequentially generated lineage-resricted neuronal and oligodendrocyte precursor cells in the spinal cord. *Development*. **134**, 285–293 (2007).

71. S. H. Woo, S. Ranade, A. D. Weyer, A. E. Dubin, Y. Baba, Z. Qiu, M. Petrus, T. Miyamoto, K. Reddy, E. A. Lumpkin, C. L. Stucky, A. Patapoutian, Piezo2 is required for Merkel-cell mechanotransduction. *Nature*. **509**, 622–626 (2014).

72. L. Madisen, T. A. Zwingman, S. M. Sunkin, S. W. Oh, H. A. Zariwala, H. Gu, L. L. Ng, R. D. Palmiter, M. J. Hawrylycz, A. R. Jones, E. S. Lein, H. Zeng, A robust and high-throughput Cre reporting and characterization system for the whole mouse brain. *Nat. Neurosci.* **13**, 133–140 (2010).

73. L. Madisen, T. Mao, H. Koch, J. M. Zhuo, A. Berenyi, S. Fujisawa, Y. W. A. Hsu, A. J. Garcia, X. Gu, S. Zanella, J. Kidney, H. Gu, Y. Mao, B. M. Hooks, E. S. Boyden, G. Buzsáki, J. M. Ramirez, A. R. Jones, K. Svoboda, X. Han, E. E. Turner, H. Zeng, A toolbox of Cre-dependent optogenetic transgenic mice for light-induced activation and silencing. *Nat. Neurosci.* **15**, 793–802 (2012).

74. B. M. Hooks, J. Y. Lin, C. Guo, K. Svoboda, Dual-channel circuit mapping reveals sensorimotor convergence in the primary motor cortex. *J. Neurosci.* **35**, 4418–4426 (2015).

75. J. M. Gee, N. A. Smith, F. R. Fernandez, M. N. Economo, D. Brunert, M. Rothermel, S. C. Morris, A. Talbot, S. Palumbos, J. M. Ichida, J. D. Shepherd, P. J. West, M. Wachowiak, M. R. Capecchi, K. S. Wilcox, J. A. White, P. Tvrdik, Imaging Activity in Neurons and Glia with a Polr2a-Based and Cre-Dependent GCaMP5G-IRES-tdTomato Reporter Mouse. *Neuron*. **83**, 1058–1072 (2014).

76. N. Choi, B. Zhang, L. Zhang, M. Ittmann, L. Xin, Adult Murine Prostate Basal and Luminal Cells Are Self-Sustained Lineages that Can Both Serve as Targets for Prostate Cancer Initiation. *Cancer Cell*. **21**, 253–265 (2012).

77. D. Voehringer, H.-E. Liang, R. M. Locksley, Homeostasis and Effector Function of Lymphopenia-Induced "Memory-Like" T Cells in Constitutively T Cell-Depleted Mice. *J. Immunol.* **180**, 4742–4753 (2008).

78. T. Buch, F. L. Heppner, C. Tertilt, T. J. A. J. Heinen, M. Kremer, F. T. Wunderlich, S. Jung, A. Waisman, A Cre-inducible diphtheria toxin receptor mediates cell lineage ablation after toxin administration. *Nat. Methods*. **2**, 419–426 (2005).

79. K. A. Christensen, J. T. Myers, J. A. Swanson, pH-dependent regulation of lysosomal calcium in macrophages. *J. Cell Sci.* **115**, 599–607 (2002).

80. L. Chen, K. Lai, J. M. Lomask, B. Jiang, N. Zhong, Detection of mouse cough based on sound monitoring and respiratory airflow waveforms. *PLoS One*. **8**, 1–10 (2013).

81. A. Okazaki, J. Hara, N. Ohkura, M. Fujimura, T. Sakai, M. Abo, N. Katayama, K. Kasahara, S. Nakao, Role of prostaglandin E2 in bronchoconstriction-triggered cough response in guinea pigs. *Pulm. Pharmacol. Ther.* **48**, 62–70 (2018).

Author contributions:

Conceptualization: LFS, DJ

Methodology: LFS

Investigation: LFS

Visualization: LFS

Funding acquisition: LFS, DJ

Supervision: DJ

Writing: LFS, DJ

Competing interests: Authors declare that they have no competing interests.

Data and materials availability: All raw data, detailed protocols and MATLAB scripts in the main text or the supplementary materials are available upon request. The acquisition number for the deep sequencing data reported in this paper is GEO: tbd.

Materials and Methods

Animals
Mouse breeding, housing and use was approved by the UCSF Animal Care and Use Committee. All animals were adult aged >10 weeks, mixed gender (as we did not see an effect of gender in our studies), housed in groups and on a C57BL/6 background. Mice were maintained in 12hr light/dark cycle with food and water provided *ad libitum*.

The following mice have been previously described and are publicly available from The Jackson Laboratory: *Ascl1^{CreERT2}*(#012882, (*70*)), *Piezo2$^{flox/flox}$* (#027720, (*71*)), *Piezo2$^{tm1.1(Cre)}$* (#027719, (*71*)), Ai14 (*Rosa26$^{LSL-tdTomato}$*, #007914, (*72*)), Ai32 (*Rosa26$^{LSL-Channelrhodopsin-2}$*, #024109, (*73*)), ReaChR (*Rosa26$^{LSL-ReaChR}$*, #024846, (*74*)), PC:GCaMP5G-tdTomato (*75*), Krt8-CreER^{T2} (#037269, (*76*)), DTA (*Rosa26$^{lsl-DTA}$*), #009669 (*77*), and DTR (*Rosa26^{iDTR}*), #007900 (*78*). We used PC:GCaMP5G-tdTomato because we could not easily identify NE cells with only GCaMP expression, as they are rare cells with low basal fluorescence of GCaMP. Genotyping was performed on lysed tail clippings with standard protocols available from The Jackson Laboratory. Cre-negative littermates were used as controls for optogenetics experiments.

Tamoxifen induction of Cre recombination
Tamoxifen (Sigma-Aldrich #T5648) was batch prepared by diluting 20 mg/mL in corn oil (Sigma #C8267) in sterile conditions. Tamoxifen was rotated at 37°C overnight in the dark before being aliquoted at stored at -20°C. Intraperitoneal (i.p.) injections of 4 mg (200 µL) tamoxifen were delivered in mice over 20 g bodyweight. For mice under 20 g, we used 2x doses of 2 mg/20 g body weight spaced by 2 days. Unless otherwise stated, mice were used within three weeks after tamoxifen injection. For optogenetics, *Piezo2* knock-out and NE cell ablation experiments, all experimental and control animals received 3x 3 mg tamoxifen with 1-2 days between i.p. injections.

Tissue dissection, fixation and immunohistochemistry staining
All mice were euthanized with carbon dioxide (CO_2) gas and tissue was harvested after perfusion of ~10 mL PBS into the right cardiac ventricle. Thoracic organs were dissected from the animal with dissecting scissors placed flush with the base of the skull to preserve the larynx.

Lobes of the lung were removed from the extrapulmonary bronchi and fixed in fresh 4% paraformaldehyde (PFA, Electron Microscopy Sciences #15710) overnight at 4°C and washed with 2x 1 hr PBS the next day. Excess connective tissue was removed from the trachea and larynx, then the airway was transected along the length of the trachealis muscle then pinned down on a Sylgard dish (World Precision Instruments #sylg184) using insect pins (Fine Science Tools, #26000-25). The dish was flooded with fresh 4% PFA for 1 hr at 4°C before the airway was unpinned and washed 2x with PBS for 2 hrs at room temperature.

For preparing cryosectioned slices, tissues were cryopreserved in 30% sucrose at 4°C for one day (larynx/trachea) or two days (lung). Tissues were blotted on a kimwipe and embedded in Tissue-Tek® O.C.T. (Sakura, #4583) in a cryomold (Electron Microscopy Sciences, #62534-10) and frozen on dry ice. Blocks were stored at -80°C until cryosectioning. Coronal sections of the lung or larynx/trachea were cryosectioned at -20°C using a Leica CM 30503 cryosectioner to cut 20 µm slices onto superfrost plus microscope slides (Fisher #12-550-15) with 6-8 sections per slide. For

images of neuron-NE cell interactions, 40 μm slices were cut. Henceforth, slides were protected from light. Slides were dried at room temperature for 2 hrs before being stored for up to 3 months at -20°C. Slides at RT were washed 2x PBS for 5 min, permeabilized with 0.2% Triton-X in PBS for 20 min, blocked with 5% normal goat serum/0.3% Triton-X in PBS (blocking buffer) for 1-2 hr. Slides were incubated with primary antibody in diluted blocking buffer (1:1 blocking buffer:PBS) overnight at 4°C. The next day they were washed 3x with 0.2% Triton-X in PBS for 10 min at RT, incubated with secondary antibody (1:500) and DAPI (1:1000) in diluted blocking buffer for 1-2 hrs at room temperature, washed in 0.2% triton-X in PBS for 10 min and washed 2x in PBS for 5 min. PBS was removed and prolong gold antifade (Thermo Fisher #P36931) was added along with a coverslip (Fisher #12-548-5M). For wholemount immunostaining of the trachea/larynx, a similar protocol was used except washes were 4 hrs, blocking was overnight, primary antibody was incubated for 2 days and secondary antibody was incubated for 1 day.

Primary antibodies used were anti-CGRP (Goat, abcam #ab36001, 1:250), anti-CGRP (Rabbit, Sigma #C8198, 1:500), anti-5HT (Rabbit, ImmunoStar #20080, 1:500), anti-PGP9.5 (Rabbit, Abcam #ab10404, 1:500), anti-PGP9.5 (Guinea pig, Abcam #ab10410, 1:500), anti-Tuj (Rabbit, Abcam #ab18207, 1:500), anti-Spp1 (Goat, R&D systems, AF808) and anti-Cartpt (Rabbit, Phoenix Pharmaceuticals #H-003-62, 1:2500). Secondary antibodies were a combination of anti-Goat, anti-Rabbit, anti-Guinea pig IgG H&L Alexa Fluor in 488, 568 and 647 channels (Sigma, 1:500).

Microscopy and imaging

Confocal imaging was performed in the UCSF Nikon Imaging Core. All cryosectioned samples were imaged using a Nikon Ti inverted microscope with Andor Borealis CSU-W1 Spinning Disk and Andor Zyla 4.2 cMOS camera. 20 μm cryosections were imaged using 60x (Nikon, oil, NA = 1.4) or 100x (Nikon, oil, NA = 1.4) immersion objectives. 40 μm cryosections were imaged using 40x (Nikon, air, NA = 0.95) objective. Images shown in figures are FIJI maximum z projections, except when otherwise stated. Quantification of histological overlap of antibodies was done in FIJI by analyzing single image planes. Whole mount samples were imaged using a Nikon Ti inverted microscope with DS-Qi2 monochrome camera, Sutter Lambda LS-2 xenon arc lamp and Sutter Lambda 10-3 filter changer and a Nikon 10x air objective (NA = 0.45). For quantification of NE cell density, images were collected by imaging the medial sections of the bronchi, lower trachea (2-4 tracheal rings from carina), middle trachea (8-9 rings from carina), upper trachea (1-2 rings from cricoid cartilage) and larynx (subglottis) and then cells were manually counted in FIJI. For quantification of NE cell ablation, only images of the subglottal larynx were acquired.

Microdissection of pulmonary NE cells from precision cut lung slices

Pulmonary NE cells are extremely rare in whole lung lysate so to decrease FACS sorting time and increase the health of dissociated cell cultures, we manually enriched for NE cells from neuroepithelial bodies (NEBs). We first made precision cut lung slices. After euthanizing and perfusing the animal as described above, we surgically exposed the trachea and threaded a 4-0 suture (Henry Schein 5610810) in a loose knot around the trachea and esophagus midway down the trachea. Using fine dissecting scissors (FST 15000-00) we cut a small hole in the trachea just anterior to the suture knot and inserted a cannula (Jelco IV Catheter, 20G, 1-1/4", #4056) into the airway. We then slowly instilled 1-2 mL of melted 2% low melting point agarose (Sigma-Aldrich A4018) into the lung stopping once the lobes were full. We covered the lobes of the lung with cold PBS, tightened the suture knot as we removed the cannula and then dissected out all thoracic

organs and placed them in cold PBS. Individual lobes were then removed and adhered to a 2-5 cm thick block of 2% agarose that was adhered to a vibratome puck. We then cut 200 µm coronal lung slices with a Leica VT 1000S vibratome. Clusters of pulmonary NE cells were identified and dissected under a fluorescent microscope with fine dissecting scissors then collected in an Eppendorf tube.

Fluorescence Activated Cell (FAC) sorting
All cells used for sequencing were from $Ascl1^{CreERT2}$; $Rosa26^{LSL-TdTomato}$ animals and, in parallel, we prepared tissue from WT animals for null and single channel FACs controls. For all dissections we asphyxiated animals with CO_2 and perfused the right cardiac ventricle with PBS. We dissected the trachea from the carina to the second most anterior tracheal ring with careful removal of the trachealis muscle. The larynx was defined as the region inferior to the pharynx and superior to the trachea, with external cartilage, muscles, bones and thyroid tissue carefully removed. Before dissociation, the trachea and larynx were coarsely cut into smaller pieces in an Eppendorf tube. When sorting pulmonary NE cells, we manually enriched for NEBs as described above.

For dissociation, tissue was incubated in 500 µL of filtered papain solution for 15 min at 37°C, then 500 µL of filtered collagenase/dispase solution for 15 min at 37°C. Papain solution was 3% papain suspension (Worthington LS003126), 0.2% saturated sodium bicarbonate (Sigma-Aldrich S5761) and 0.667 mg/L L-cysteine (Sigma #C7352) in phenol red-free HBSS (Cytiva SH30268.01). Collagenase/dispase solution was 4 mg/mL collagenase Type 2 (Worthington LS004176) and 4.7 mg/mL dispase II (Sigma-Aldrich D4693) in phenol red-free HBSS. After dissociation, we centrifuged the samples at 200 g for 3 min, removed supernatant and then added 1 mL of quench solution: 10% FBS (R&D systems S11650H), 2mM EDTA and 0.5 µg/mL DNAse (Sigma, #DN25). We gently triturated the quench solution with a 1000 mL pipette and then a 200 µL pipette. Large pieces of cartilage and agarose that blocked the pipette were removed and sample was slowly strained through a 100 µm filter (BD 352360) into an Eppendorf tube. We centrifuged the samples at 200 g for 3 min, removed the supernatant, and resuspended with sort buffer: HE Buffer A, 2% FBS, 1x GlutaMAX and 2 mM EDTA. We then stained the cells with 1:100 CD45-450 (ThermoFisher 11-0451-82), 1:400 EpCam-Cy7 (ThermoFisher 25-5791-80) and 5 nM SyTox Red Dead Cell Stain (ThermoFisher S34859) for 30 min at 4°C. Experimental samples were washed with sort buffer twice and then resuspended with sort buffer containing 1:100 Ribolock (Thermo Fisher Scientific EO0382) and SytoxRed.

Airway epithelial cells were sorted in the Laboratory for Cell Analysis at UCSF by fluorescence-activated cell soring (FACS) using an Aria II flow cytometer (BD Biosciences) with an 85 µm nozzle. After calibrating lasers with unstained and single channel control samples, we sorted NE cells (SyTox-/CD45-/EpCam+/TdTomato+) and an equal number of epithelial control cells (SyTox-/CD45-/EpCam+/TdTomato-). For tracheal and laryngeal NE cells, we sorted 500 cells per replicate. For pulmonary NE cells, we sorted 1000 cells per replicate. Cells were sorted into 9.5 µL of 1x Takara SmartSeq v4 lysis buffer with 1x ribolock. Sorting of experimental cells took 15-20 min and generated an additional ~1 µL of liquid. Samples were spun down and flash frozen in an ethanol dry ice bath and stored at -80°C. Finally, we sorted 100 NE cells into 9.5 µL of sort buffer and verified cell health and tdTomato+ identity using a fluorescent microscope.

RNA sequencing and analysis
We collected three biological replicates on different days, but generated cDNA libraries in parallel. We followed the Takara Smart-Seq v4 ultra low input RNA protocol with the following modifications. Samples were adjusted to 10.5 µL at the start of generating a cDNA library and then 2 µL of 3' SMART-seq CDS Primer II A was added. We empirically determined that 12 rounds of amplification were appropriate for 500-1000 airway epithelial cells, including NE cells. PCR product was purified with AMPure XP beads (Beckman Coulter A63880). We used Agilent High Sensitivity DNA Kit (Agilent Technologies 5067-4626) to quantify the amount of DNA (pg/µL) between 400-7000 bp and qualitatively assess that the library was a broad peak with no spikes of overamplification. cDNA libraries were stored at -20°C.

We next finished cDNA library preparation with the following modifications to the Nextera XT protocol (Illumina FC-131-1001). For tagmentation, we diluted 100 pg of cDNA in 2 µL of RNAse free water, added 2.5 µL TD and 0.5 µL ATM buffers, then incubated for 7 min at 55°C. We then added 0.5 µL NT buffer and incubated for 5 min at room temperature then placed samples back on ice. For library indexing and amplification, we added the following to the tagmentation reaction: 1.2 µL primer 1, 1.2 µL primer 2, 0.5 µL water and 3.6 µL MasterMix NPM. After PCR amplification, we used the High Sensitivity Bioanalyzer to quantify the concentration between 200 – 1000 bp and qualitatively assessed that it was a broad hump. We combined equimolar concentrations of each sample together and then added 1.2x of the final sample volume of AMPure XP beads. Briefly, to purify we incubated the sample at room temperature for 8 min, washed the beads twice with 200 µL of fresh 80% ethanol, removed all ethanol, dried the beads for 2 min, then resuspended with 30 µL of Nextera XT Resuspension Buffer. We used the bioanalyzer to quantify the final combined product. Tracheal and laryngeal NE and epithelial cells were sequenced with Illumina Hi-Seq 4000 platform at the UCSF Center for Advanced Technology with single end reads to a depth of 38-45 million reads per sample. Quality control and adapter trimming was performed with Cutadapt and FastQC using TrimGalore (https://github.com/FelixKrueger/TrimGalore). Reads were aligned to the mouse reference genome (mm10 with the sequence for tdTomato added) using StarAlign and reads were counted using the rsem-calculate-expression function of RSEM-1.3.3. Data are either presented as transcripts per million reads (TPM) or log2 adjusted TPM. We did not perform statistical analysis on sequencing data, but rather used it to generate experimental hypotheses.

Whole-cell patch-clamp electrophysiology
Recordings were carried out at room temperature using a MultiClamp 700B amplifier (Axon Instruments) and digitized with a Digidata 1550B (Molecular Devices). Data were filtered at 1 kHz and sampled at 10 kHz. Membrane potentials were corrected for liquid-junction potential after data collection. For dissociated cells, cells were visualized with an Olympus 1X71 inverted microscope and Lamda DG-4 light source (Sutter Instruments). For *ex vivo* preparations, cells were visualized with an Olympus BX50W1 upright microscope. Both microscopes used Sutter MP225 micromanipulators and CV7B headstage (Axon Instruments). NE cells were identified by tdTomato fluorescence and recordings were performed with thick-walled borosilicate glass pipettes (BF-150-86-10) fire polished to a resistance of 8-10 MOhm using a Micro-forge MF-830 polisher. All recordings were performed with a standard Kreb's extracellular solution which contained (mM): 140 NaCl, 3 KCl, 1.8 $CaCl_2$, 1 $MgCl_2$, 10 HEPES, 5 Glucose, pH to 7.2 using NaOH with an approximate osmolarity of 290 mOSM. Intracellular saline contained (mM): 140 K-gluconate, 5 NaCl, 1 $MgCl_2$, 0.02 K-EGTA, 10 HEPES, 10 Sucrose, pH to 7.2 using KOH with an approximate osmolarity of 290 mOSM. Recordings were only used if they reached >20 GOhm

seal before breaking in. We did not normalize to capacitance (pF), as it is difficult parameter to accurately measure in very small cells, but pulmonary, tracheal and laryngeal NE cells appear the same size and all have approximate capacitance measurement between 2-3 pF. For voltage clamp recordings, cells were kept at a holding potential of -80 mV and currents were elicited by 100 ms voltage steps in 10 mV increments between -100 to +90 mV. For current clamp recordings, cells were held with 0 pA of current and current was injected into the cell during 800 ms steps. For some calcium imaging recordings, cells were held at -80 mV and stepped to -35 mV and 0 mV for 1000 ms, returning to -80 mV between pulses. For pharmacology experiments the following blockers were used (in μM): 0.5 tetrodotoxin (Cayman Chemical Company #14963), 10 mM tetraethylammonium (Sigma #86614), 100 4-aminopyridine (Tocris #0940), and 10 XE991 (Tocris, #2000). For identification of two pore potassium channel currents, the following external saline was applied on the cell in the presence of TTX, TEA, 4-AP and XE991 (in mM): 5 NaCl, 140 KCl, 1.8 $CaCl_2$, 1 $MgCl_2$, 10 HEPES and 5 Glucose, pH adjusted to 7.2 with KOH.

For *Piezo2*-conditional knock out (cKO) studies, dissected animals ~one month after the third tamoxifen injection. NE cells from WT ($Ascl1^{CreERT2}$; $R26^{lsl-tdTomato}$; $Piezo2^{+/+}$) and cKO ($Ascl1^{CreERT2}$; $R26^{lsl-tdTomato}$; $Piezo2^{fl/fl}$) animals were dissociated in parallel enabling us to be blinded to the genotype of cells we patched onto.

Ex vivo lung and tracheal tissue preparation

150-200 μm precision cut lung slices were prepared as described above. Intact slices were pinned with 2-3mm x 20 μm tungsten wire pins to sylgaurd in a dish. We often had to remove a single layer of cells to access the pulmonary NE cell. For tracheal NE cell recordings, tracheal rings were dissected, cut open at the trachealis muscle, oriented along the sagittal plane such that all epithelial cells were facing up and then pinned to sylgaurd in a dish. Whole-cell patch-clamp electrophysiology was performed as described above.

Dissociated NE cell preparations

NE cells from $Ascl1^{CreERT2}$; $R26^{LSL-tdTomato}$ mice were dissociated as described above for FACS sorting, except that after adding quench buffer and titurating with a pipette, 1 mL of DMEM was added, the cells were gently spun down (200 g), supernatant was removed and then the cells were again re-suspended with 100 μL of DMEM per coverslip (ex. use 800 μL for plating onto 8 coverslips). 100 μL of cell suspension was plated on 12 mm round coverslips (Bellco Glass 194310012A) that were coated in laminin (Invitrogen 23017015). For laminin coating, ethanol-sterilized coverslips were dried in a petri dish and then 100 μL of 10 μg/mL laminin diluted in 0.5% poly-D lysine was added and incubated at 37°C, 5% CO_2 for 4 hrs. Coverslips were washed 3x with sterile water and 3x with DMEM. Cells were plated and incubated at 37°C, 5% CO_2 for 2 hr, then placed in 12 well dishes with pre-warmed advanced DMEM/F12 containing 10% FBS, 1% penicillin/streptomycin and 1x GlutaMAX. Cells were left overnight in 37°C, 5% CO_2 incubator then patched the next day. For mechanical sensitivity experiments, cells were patched on day 2. For experiments using dissociated cells from extrapulmonary bronchi, tissue was dissected from the carnia to the lung lobe and then dissociated.

ATP Biosensor Recordings

HEK293T (ATCC) were grown in DMEM, 10% fetal bovine serum and 1% penicillin/streptomycin at 37°C, 5% CO_2. Cells were seeded at a density of 0.2-0.25x10^6 cells per well in a 24 well plate and 14 hrs later transfected ATP1.0 plasmid (Addgene #167582, 29) with Lipofectamine 3000 (Thermo Scientific L3000008) following the manufacturer's protocol. Cells

were grown at 37°C, 5% CO_2 for 10 hrs and then 30°C, 5% CO_2 for 38 hrs. Cells were briefly trypsinized with the reaction quenched by DMEM with 10% FBS. Cells were resuspended in ~400 µL of external saline and then ~30 µL of the suspension was gently pipetted above an area of the coverslip containing dissociated NE cells from $Ascl1^{CreERT2}$; $R26^{LSL- tdTomato}$ mice. We adhered a brightly fluorescent cell to a large bore electrode filled with external saline and then used a micromanipulator to gently move it directly next to a NE cell. We then measured changes in fluorescence in the ATP1.0 biosensor cell. For pulse experiments, we patched onto the NE cells and then pulsed to -70 mV and -10 mV at 5 Hz with a 100 ms pulse width for 4 s. For experiments investigating mode of ATP release, dissociated NE cells were incubated in either 100 µM [10]panx or Krebs external saline (see above) without Ca^{2+}/Mg^{2+}. As a positive control, Krebs external saline with Ca^{2+}/Mg^{2+} was used at the end of all experiments to ensure pulsing to -10 mV still drove ATP release. For high potassium (high-K) and water experiments, we placed ATP1.0 biosensor cells next to both NE cells or other dissociated non-NE cells. For a given trial, we continuously perfused external saline over the cells (which causes a gradual decrease in fluorescence) and then pulsed external saline, high-K or water and finally 10 µM ATP (Sigma #A6419) over cells. ATP is prepared fresh daily. We simultaneously recorded the TTL pulse from the DG4 and smartsquirt using a Digidata 1550B (Molecular Devices) so we could align the electrophysiological or smartsquirt pulses with the ATP1.0 biosensor movie collected in micromanager.

Fura Imaging in Dissociated Cells
Dissociated NE cells from $Ascl1^{CreERT2}$; $R26^{LSL- tdTomato}$ mice were loaded with 10 µM Fura-2-AM (Invitrogen) and 0.01% Pluronic F-127 for 1 hr in Kreb's external saline. Experiments were conducted on the Olympus 1X71 inverted microscope and 340 nm and 380 nm images were captured sequentially at a rate of ~5 Hz using custom settings on micromanager. NE cells were stimulated with high potassium consisting of (in mM): 3 NaCl, 140 KCl, 1.8 CaCl2, 1 MgCl2, 10 HEPES and 5 Glucose, adjusted to pH 7.2 with KOH, ~290 mOSM.

For Ca_V channel blocker experiments we stimulated the cell with high-K (baseline high-K), exchanged external saline, waited 10 min, stimulated again with high-K (control high-K), exchanged with channel blocker, waited 10 min, then stimulated with high-K (blocker high-K). Using FIJI, the cell's fluorescence was background corrected and then the ratio of 340 nm to 380 nm was calculated: $((340_{Cell} - 340_{Background})/ (380_{Cell} - 380_{Background}))$. Control and blocker high-K were expressed as a percentage of baseline high-K. We used the following Ca_V blockers (µM): 10 nifedipine (Alomone Labs N-120), 0.3 ω-agatoxin IVA (Tocris, #2799), 5 mibefradil (Tocris, #2198), and 10 NNC-55-0396 (Cayman Chemical #17216).

When imaging calcium responses to acid in dissociated cells, there were several technical artifacts that result in delayed Fura response after low pH was washed off. Given that we know acid-evoked calcium entry depends on activation of T-type voltage-gated calcium (Ca_V) channels, we present the following explanation for the delayed responses. First, perfusion of pH2 solution immediately bathes the cell's entire membrane in a solution that completely inhibits voltage-gated calcium (Ca_V) and sodium (Na_V) channels and results in partial inhibition of potassium channels. Immediate inhibition of Ca_V channels explains why we do not observe (1) an immediate calcium response upon perfusion of pH2 solution as we do in ex vivo explants and (2) why we do not see a calcium response when dissociated cells are depolarized due to inhibition of potassium channels. Next, hydrogen ions gradually enter the cell during pH 2 perfusion, which is reflected by a gradual decrease in the Fura ratio due to an increase in Fura's dissociation constant (Kd), as the Kd is

known to increase by several orders of magnitude between pH 7 and pH 4 (*79*). Using electrophysiology, we then determined that when pH 2 solution is washed off, the membrane potential bounces above and below threshold for activation of T-type Ca_V channels. This is likely due to a technical artifact of perfusing solutions in a bath. We believe that in this time frame, T-type calcium channels are activated resulting in calcium influx. However, because hydrogen ions have not been fully pumped out of the cells, Fura is still only weakly binding the calcium. Once internal pH increase, the residual calcium signal is revealed. These technical artifacts are unique to dissociated cells, because in intact tissue, only a small part of the membrane of NE cells will be directly exposed to any perfused solution.

Due to these technical artifacts, we imaged and analyzed acid responses in dissociated cells in the following manner with each frame exposed for 100 ms and ultimately a period of 120 ms between frames due to delay in opening/closing the shutter. Perfusion: 0-100 frames external solution (turn external solution off/on at frames 40 and 90 to mimic pulsing solutions), 100-150 frames pH2, 150-400 frames external saline, 400-425 frames high potassium and 425-500 frames external saline. We calculated the change in Fura Ratio at the following points. Ext: baseline (frame 40) and peak response (peak of frames 50-90). pH2: baseline (frame 100) and peak response (peak of frames 210-250). high-K: baseline (frame 400) and peak of response (peak of frames 410-430). Data are presented at change in Fura ratio (Peak – Baseline). For trials where we inhibited T-type Ca_V channels, cells were continuously bathed in 10 uM NNC-55-0396 with a pre-incubation step of 5 min.

Ex vivo NE cell calcium imaging with GCaMP
All mice were $Ascl1^{CreERT2}$; $Polr2a^{LSL-GCaMP5G, tdTomato}$. 150-200 um lung slices were cut, described as above, and adhered to the bottom coverslip of an imaging chamber (Warner Instruments JG-23) using small amounts of super glue applied along the outside edge of the lung slice 2-3 cm from any NE cell being imaged. Tracheal rings and pieces of the larynx were oriented in the transverse plane and then adhered to the bottom coverslip of an imaging chamber using small amounts of super glue applied to the outside cartilaginous part of the airway. We then imaged GCaMP responses using an Olympus 1X71 inverted microscope. Imaging along the transverse plane allowed us to image almost the whole NE cell from tip to basal side. Imaging cells close to the coverslip with an inverted microscope maximized stability of the cell in the focal plane when solutions were applied, especially water which causes the tissue to expand. Images were collected at a frame rate of 10 Hz.

Low pH external saline consisted of (in mM): 140 NaCl, 5 KCl, 25 Citric Acid, 1 MgCl2 and 2 CaCl2, pH was ~2.3 and 290 mOSM. Water consisted of 10 mM HEPES to allow for maintenance of a neutral pH and 2 mM CaCl2. Stimuli were applied using a SmartSquirt (Automate Sciences) with 100 μm applicator nozzle.

Dissociated NE Cell Calcium imaging with GCaMP
We dissociated tissues from $Ascl1^{CreERT2}$; $Polr2a^{LSL-GCaMP5G, tdTomato}$ mice as described above and performed all experiments on an Olympus 1X71 inverted microscope. For experiments where we performed dual patch-clamp electrophysiology and imaging, electrophysiological measurements were collected as described above. To facilitate precise analysis, a TTL pulse from the SmartSquirt box and from the DG4 fed into the digitizer. The DG4 TTL pulse designated when the shutter opened and closed and the SmartSquirt TTL pulse designated which channel was turned on or off, which was then aligned to the electrophysiology recording.

We used the following external salines for pH and osmolarity experiments. For all pH experiments external salines had (in mM): 140 NaCl, 5 KCl, 1.8 $CaCl_2$, 1 $MgCl_2$. pH 5.5 and 6.5 had (in mM): 10 MES and 5 Glucose, pH was adjusted with NaOH. pH 4 (in mM): 10 Citric Acid, 5 Glucose, pH was adjusted with NaOH. pH 2 (in mM): 25 Citric Acid.

Piezo2 cKO studies ($Ascl1^{CreERT2}$; $Polr2a^{LSL-GCaMP5G, tdTomato}$, $Piezo2^{fl/fl}$), NE cells were dissociated from the lung and trachea of the same mice to provide an internal control for success of *Piezo2* KO. As with electrophysiology, cKO and WT animals were treated with tamoxifen and then NE cells were dissociated 4 weeks later.

Vagal nerve *ex vivo* recordings
All animals used were littermate progeny from $Ascl1^{CreERT2/+}$ crossed to either homozygous $Rosa26^{LSL-ReaChR}$ or $Rosa26^{LSL-ChR2}$. Mice were euthanized with CO_2 and perfused the right cardiac ventricle with PBS. We then carefully dissected out all thoracic organs with the main vagus nerve fibers attached. We next removed the heart, thymus, fat, lobes of the lung and main vagus nerve fiber with careful monitoring of the recurrent and superior laryngeal nerve (RLN, SLN) fibers to ensure they were not disrupted. The RLN was cut at the point when it separated from the vagal nerve fiber at the inferior end of the trachea. Using fine dissecting scissors (FST 15000-00), we transected the anterior trachea through the cartilage rings and then used insect pins (FST 2600130) to pin down the flayed trachea on a sylgaurd dish bathed in Kreb's external saline. We then desheathed the RLN and superior laryngeal nerve (SLN) and let the preparation rest in the dark at room temperature for 30 min before beginning recordings.

For whole nerve electrophysiology, we pulled a long, finely tapered sharp electrode (1.5 OD/0.84ID, World Precision Instruments #1B150-4) using a P-97 Sutter instrument puller. The electrodes were broken near the base of the tip to be the size of the RLN or SLN and then attached to head stage. External saline was suctioned into the electrode with ground electrode placed in the bath. Then either the RLN or SLN was suctioned into the electrode. Nerve activity was detected with a differential AC amplifier (AM-systems Model 1800) with a low cut off of 100 Hz, high cut-off of 1000 Hz and gain of 10k. Output was digitized by Digidata 1550B (Axon Instruments). Signal was recorded in Clampex 11.2 at a sampling rate of 10 kHz.

The laser/light guide were placed above preparation at defined locations. We used a 532nm laser (WSLS-532-020m-H, WSLaser-D500440) without a light guide for ReaChr experiments and a 473 nm laser (Opto Engine LLC, MBL-F-473-200mW, DF60513) with a light guide (Doric, D207-1239-0.4) for ChR2 experiments. All components near the electrode holder were shielded in tin foil and grounded to minimize electrical noise. In each trial we collected data for the 50 s before, during and after optogenetic activation (10 Hz with 50 ms pulse width). Laser was controlled by TTL pulse from digitizer. We let the preparation rest for 30 min between trials. Compound action potentials (CAPs) were calculated with custom MATLAB scripts. Briefly, we parsed the recordings into individual waveforms, set a preparation-dependent noise threshold and then calculated the number of waveforms with peaks above that threshold, which we defined as CAPs.

Fresh preparations were used for baseline recordings in pharmacology experiments. For experiments where we used a high salt stimulus, we added high salt (in mM: 650 NaCl, 3 KCl, 1.8 $CaCl_2$, 2 $MgCl_2$, 10 HEPES and 5 glucose, pH 7.2) 5 minutes after optogenetic stimulation and quantified the number of CAP in the first minute after application. We then exchanged the external

bath 10 times with either control saline or 50 μM PPADs (a broad P2x receptor antagonist, Tocris, #0625), incubated for 30 min and then collected a second recording. Quantification was made by the ratio of the number of compound action potentials (CAPs) in the experimental condition (control or saline) vs baseline CAPs.

Whole animal optogenetics

$Ascl1^{CreERT2}$; $Rosa26^{LSL-ChR2}$ animals were used one week after tamoxifen administration. Mice were anesthetized with urethane (1.5-1.8 mg per gram body weight). We observed that faster, presumably deeper, anesthesia led to fewer optogenetics evoked swallowing reflexes and almost complete loss of post-swallow expiratory and cough-like reflexes, which is consistent with the common observation that different depths of anesthesia change evoked reflexes. Thus, mice were given 1.5 mg/g urethane and we only used mice that took >1 minute to become unresponsive to toe pinches. If they did not lose their toe pinch reflex after 10 min, the urethane dosage was increased to 1.8 mg/g. Urethane powder was kept in desiccator because we found that it became more potent when water was absorbed.

Mouse limbs were taped to a flat board and the neck was surgically exposed with sutures threaded through the thymus and taped to board. The trachea and cricothyroid membrane of the larynx were then surgically exposed with the airway remaining intact. A spirometer (AD Instruments, FE141 and MLT1L) was attached to the mouse's nose and breathing was acquired at 400 kHz with a DAQ device (PowerLab 8/35 PL3508) using LabChart Software. An optical fiber was positioned over the cricothyroid membrane of the larynx, the upper trachea (three ligaments below larynx), the middle trachea just above the sternum or the arytenoid muscles proximal to the exposed larynx. The optical fiber was connected 473nm DPSS laser (Shanghai Laser & Optics Century BL473T8-150FC) which was controlled by TTL pulse generator (Doric lenses) using Doric Studios software. For each trial we did three 10 s long pulses at 8 Hz with 100 ms pulse width with 10 s between pulses. We counted the total number of swallows, swallows with expiration reflex and cough-like reflexes for the three 10 s windows before or during stimulation.

Each reflex was characterized and identified in the following way. As breath shape and size is highly stereotyped under anesthesia, we used custom MATLAB scripts to parse each individual breath and calculate the following parameters: peak inspiratory flow (PIF), peak expiratory flow (PEF), breath length and length of time between breaths. Swallows were detected as an increase in the time between breaths (apnea). We confirmed the apneas were due to swallowing by (1) visual confirmation of hyoid bone movement and (2) electromyography (EMG) activity in the submental complex muscles controlling swallowing. To detect post-swallow expiration events and cough-like reflexes, we made kernel density plots of PEF for each trial. Breathing becomes stereotyped under anesthesia and the majority of breaths fell into a tight distribution ($0.82x - 1.15x$ of mean PEF breath size). We used the peak of that distribution to represent mean normal breath size and the lower and upper edges of that distribution to represent "smallest normal breath" and "largest normal breath," respectively. Post-swallow expiratory reflexes immediately followed a swallow-induced apnea and were greater than 1.3x mean peak expiratory flow (average +42% mean PEF). Cough-like expiratory reflex were expirations that were greater than 1.5x mean peak expiratory flow (average +70% mean PEF) and were directly preceded by a large inhalation corresponding to strong activation of the diaphragm muscles.

For EMG recordings, we attached a paired EMG electrode made from Teflon-coated multistranded stainless steel wires (Cooner Wire) to either the diaphragm or submental complex, which was

grounded with a small suture needle attached to a metal wire and threaded under the skin. The EMG electrodes were connected to an AC differential amplifier (A-M systems AM1800), band-pass filtered (300Hz/10kHz) and digitized with PowerLab DAQ. EMG recording were synchronized with breathing data. Custom Matlab scripts were used to plot the raw and integrated EMG data.

Stimulus-evoked Swallowing Assay
To test if airway NE cells contribute to the stimulus-evoked swallowing reflex, we used two diptheria toxin-based genetic strategies to deplete NE cells: Cre-dependent expression of the diphtheria toxin fragment ($Rosa26^{LSL-DTA}$) or the diphtheria toxin receptor ($Rosa26^{LSL-DTR}$). To generate littermate control and experimental progeny, mice heterozygous $Ascl1^{CreERT2/+-}$ and homozygous for lsl-tdTomato (Ai14) were crossed to mice homozygous for lsl-DTA or lsl-DTR. For DTA experiments, all mice were treated with 2 mg tamoxifen for three consecutive days and then tested a week later with the experimenter blinded to genotype. For DTR experiments, all mice were treated with 2 mg tamoxifen for three consecutive days (D1-3), then a week later treated with diphtheria toxin (DTX: 50 ng per body weight for three consecutive days (D8-10), and finally tested a week later (D15).

For the laryngeal perfusion assay we first anesthetized animals with urethane (1.5 mg/kg body weight) and only used animals that took longer than 1 min to lose responsiveness to the pinch reflex. We then taped their paws to a metal plate with the ventral side up and surgically exposed their airway using suture thread to hold open the tissue. A breathing cannula (Jelco IV Catheter, 20G) was inserted into the trachea just above the sternum. An inflow port (Radiopaque Catheter, 18G) was advanced through the mouth towards the airway until a mechanically-evoked swallow occurred. We then moved it back slightly and secured its position by sealing off the mouth and nose with a silicon sealant (World Precision Instruments, Kwik-cast). We then inserted an outflow port (Radiopaque Catheter, 18G) in the trachea two rings above where the breathing canula was inserted. The outflow port was not secured, but instead stabilized with a clay mold. We then used a peristaltic pump to deliver and remove stimuli. Experiments were terminated if there was not even flow of air/liquid out of the airways (due to clogging, leakage or poorly placed ports) as this would make it impossible to precisely control stimulus application. We also found that some DTX-treated mice (from both control and experimental groups) would have increasing difficulty breathing as the swallowing assay progressed. When this happened, the mouse was immediately euthanized (CO2 asphyxiation with cervical dislocation) and excluded from analysis.

Stimuli were perfused a constant rate of 1 mL/s and each experiment was executed in the same order. Phase 1: perfuse external saline for 10 min. Phase 2(m:ss): 0:00-0:30- air, 0:30-1:30- 3x 10 s of stimulus then 10 s air, 1:30-2:00- air, 2:00-3:00- external saline. Stimulus order: water, acid then high salt. Phase 3: perfuse 20 s air then advance the outflow port 10-11 times as a mechanical stimulus. Water was not supplemented with Ca^{2+}. High salt (in mM: 650 NaCl, 3 KCl, 1.8 CaCl$_2$, 2 MgCl$_2$, 10 HEPES and 5 glucose, pH 7.2) and pH 2 acidic solution (in mM: 140 NaCl, 5 KCl, 25 Citric Acid, 1 MgCl2 and 1.8 CaCl2, pH was ~2.3). We monitored swallowing reflexes visually or with an EMG placed in the suprahyoid muscles.

Exclusion criteria, blinding, randomization and replication
Histology: within a slide, no cells were excluded. Electrophysiology: recordings were excluded if seals did not reach >20 GOhm seal, if there was not a clean break into the cell or the seal became leaky. We generally only dissociated one tissue per day so we were not blinded to source of NE

cells except when comparing mechanosensitive currents from WT vs *Piezo2*-cKO animals. For testing mechanical sensitivity of WT vs *Piezo2*-cKOs, we dissociated pulmonary NE cells from both tissues in parallel and then were blinded to the origin of the cells on a particular coverslip until after the experiment was completed. Calcium imaging: cells whose calcium signals did not return to baseline after performing a manipulation (application of a drug, stimuli, etc) were excluded. We were not blinded to source of NE cells. Whole-nerve electrophysiology: preparations without baseline, spontaneous compound action potentials were excluded as this was indicative of technical damage to the preparation. We used littermate controls with roughly 50/50 Cre-positive or Cre-negative progeny and were blinded to genotype until after the experiment was completed. Whole animal optogenetics: No recordings were excluded, but mice that took less than 1 min to lose responsiveness to a toe pinch were immediately sacrificed (ie not experimented on). We used littermate controls with roughly 50/50 Cre-positive or Cre-negative progeny and were blinded to genotype until after the experiment was completed. Swallow assay: we only analyzed preparations where we successfully executed the whole protocol. Preparations that had a technical failure (most likely exit port falls out of trachea or difficulty breathing) in the middle of the protocol were not included. For all experiments, mice were randomly allocated from different cages of male and female mice for analyses. Exclusion criteria were preestablished and commonly used with no attrition of data during analysis.

Transcriptomic data was in three biological replicates and cells were dissociated and sorted on different days (except NE cells and epithelial cell controls were collected from the same mouse at the same time). For all electrophysiology, calcium imaging and histology experiments where *n* is defined as a cell: the cells came from at least 3 different randomly allocated mice that were dissected on different days. For histology, whole nerve electrophysiology and whole animal optogenetic experiments where *n* is defined as a preparation from an individual mouse: experiments were replicated as many times as the sample size across at least 3 different days with mice from different, randomly allocated cages.

Statistics
For whole cell electrophysiology and calcium/ATP imaging studies, all data points represent a recording from one cell, unless otherwise stated. For *ex vivo* electrophysiology, optogenetics breathing studies and the swallowing assay, all data points represent a mouse. For histology studies, representative images are based on analysis of 3-7 mice. Sample sizes were based on power calculations performed based on previous studies or pilot experiments carried out in our laboratory. We used the PRISM software package to graph and statistically analyze data. Before statistical analysis, we used the Shapiro-Wilk normality test. When data were normally distributed without large differences in variance, we used parametric tests. Otherwise, we used the comparable non-parametric test. We adjusted the *P* values accordingly when multiple tests were conducted. See Table S1 for complete details about sample sizes, normality tests, statistical tests used and *P* values.

Fig. S1

A

B — NE-associated Transcripts

C — Vesicle Release Machinery

D — Neuropeptides

E

F

G

H

I
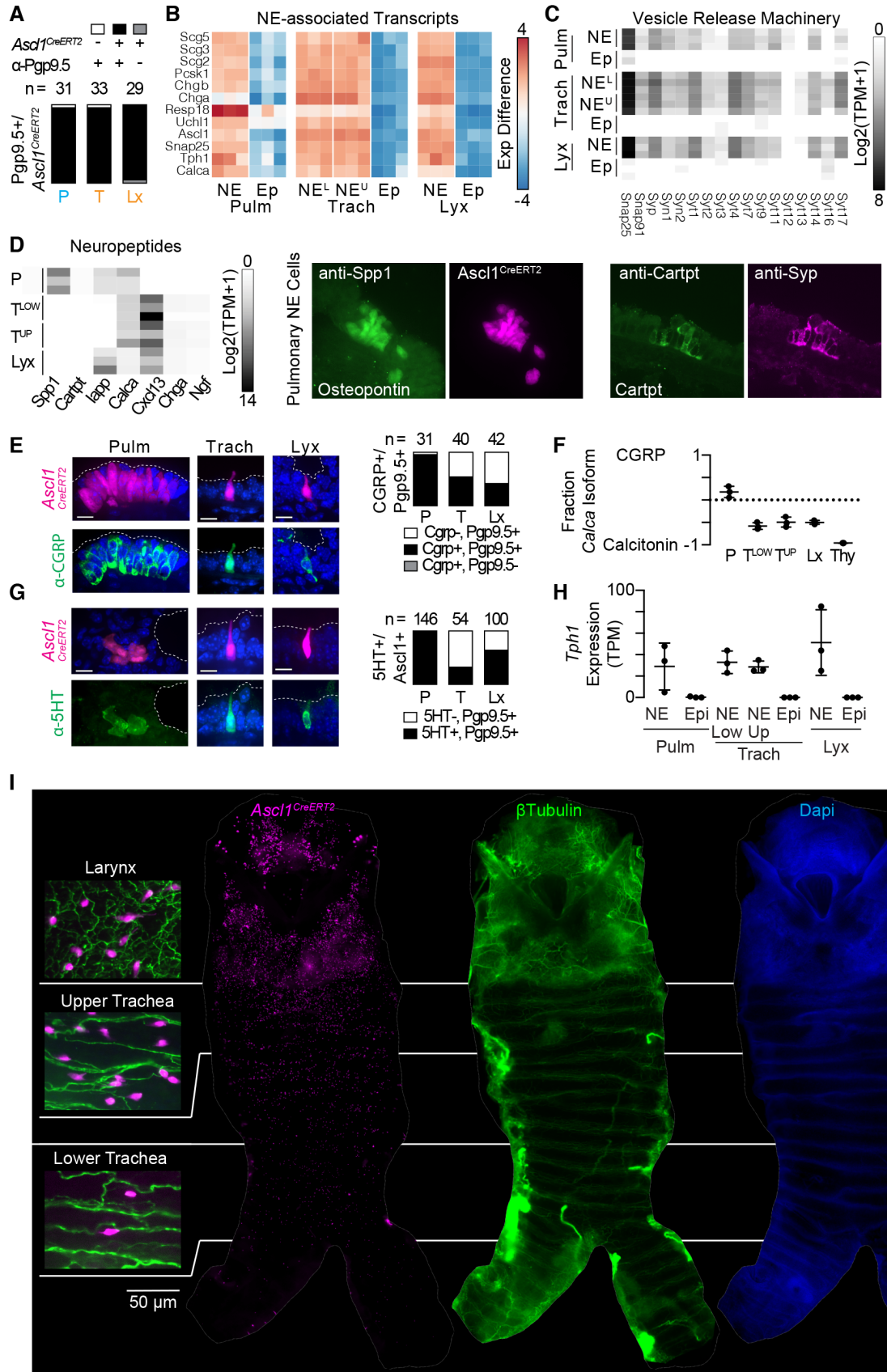
Fig. S1. Morphological diversity of neuroendocrine cells across the airway. (**A**) Fraction of epithelial cells marked by a neuroendocrine cell marker (Pgp9.5) and $Ascl1^{CreERT2}$; $R26^{lsl\text{-}TdTomato}$ in lung (P, left), trachea (T, middle) and larynx (Lx, right), black is double-positive, n is number of cells across 5 mice. (**B**) Heatmap depicting relative sample expression differences of known NE-associated transcripts by subtracting the average transcript expression (rlog transformed TPM) across all samples from each sample's transcript expression. Neuroendocrine (NE) and epithelial (Ep) cells from lung, trachea and larynx. NE^L and NE^U are NE cells from lower and upper trachea, respectively. (**C**) Expression (Log2 transformed TPM+1) for transcripts involved in vesicle release for neuroendocrine (NE) and epithelial (Ep) cells from lung, trachea and larynx. NE^L and NE^U are NE cells from lower and upper trachea, respectively. (**D**) (Left) Expression (Log2 transformed TPM+1) of highly-expressed neuropeptides in NE cells and (Right) histological validation of osteopontin and Cartpt (green) in pulmonary NE cells (pink) marked by $Ascl1^{CreERT2}$; $R26^{lsl\text{-}TdTomato}$ or anti-synaptophysin (Syp). (**E**, **G**) Co-localization of calcitonin gene related product (E, CGRP) and serotonin (G, 5-HT) in pulmonary (P), tracheal (T) and laryngeal (Lx) NE cells (pink, $Ascl1^{CreERT2}$; $R26^{lsl\text{-}TdTomato}$) with DAPI nuclear stain (blue). Quantification (right) of fraction of NE cells positive (black) or negative (white) for CGRP (E) or 5-HT (G). n is number of cells across 4 mice. (**F**) The *Calca* locus encodes distinct isoforms used to make CGRP and Calcitonin. Plotted is (# CGRP isoforms - # Calcitonin isoforms/total). -1 denotes only Calcitonin isoform, as is the case for Ascl1+ C cells of the thymus. Tracheal and laryngeal NE cells preferentially express calcitonin isoforms while pulmonary NE cells preferentially express CGRP isoforms. (**H**) Expression of essential serotonin synthesis gene *Tph1*. (**I**) Whole mount images of NE cell distribution (pink, $Ascl1^{CreERT2}$; $R26^{lsl\text{-}TdTomato}$), neural innervation (green, βTubulin) and DAPI nuclear stain (blue) across the trachea and larynx. Data are represented as means ± SDs.

Fig. S2

A

Pulmonary NE | Tracheal NE | Laryngeal NE | Neuron

B Expression of Na$_V$ Channels

Pulm | NE | Ep
Trach | NE^L | NE^U | Ep
Lyx | NE | Ep

Scn1a Scn2a Scn3a Scn4a Scn5a Scn7a Scn8a Scn9a Scn10a Scn11a

Log2(TPM+1)

C Pulmonary - Na$_V$ Current

Current (-nA)
Pre TTX Wash
ns **** **
-10 mV
nA
1 ms
0.2 nA
50 mV

D Tracheal - Na$_V$ Current

Current (-nA)
Pre TTX Wash
ns **** ****
-10 mV
nA
1 ms
1 nA
50 mV

E Laryngeal - Na$_V$ Current

Current (-nA)
Pre TTX Wash
ns **** ****
-10 mV
nA
1 ms
0.5 nA
50 mV

F

G/G$_{Max}$
-100 0mV
• Pu • Tr • Lyx

G

Expression (TPM)
P T^{L}T^{U}L P T^{L}T^{U}L
Na$_V$ 1.3 1.7

H Type of Cell: Fires Single AP Fires AP Trains

Voltage Stimulus (mV): AP Train
40
0
-60

Current Response (pA)
0
Na$_V$ Absent
Na$_V$ Present
-1000
200 ms

Na$_V$ Current after 1st AP? 0 of 6 cells 5 of 5 cells

I Na$_V$ Current

Na$_V$ Current (-nA)
4
0
AP 1 1 ≥3
Pu Tr
**** **** ****

K$_V$ Current @ 30 mV

K$_V$ Current (nA)
2.5
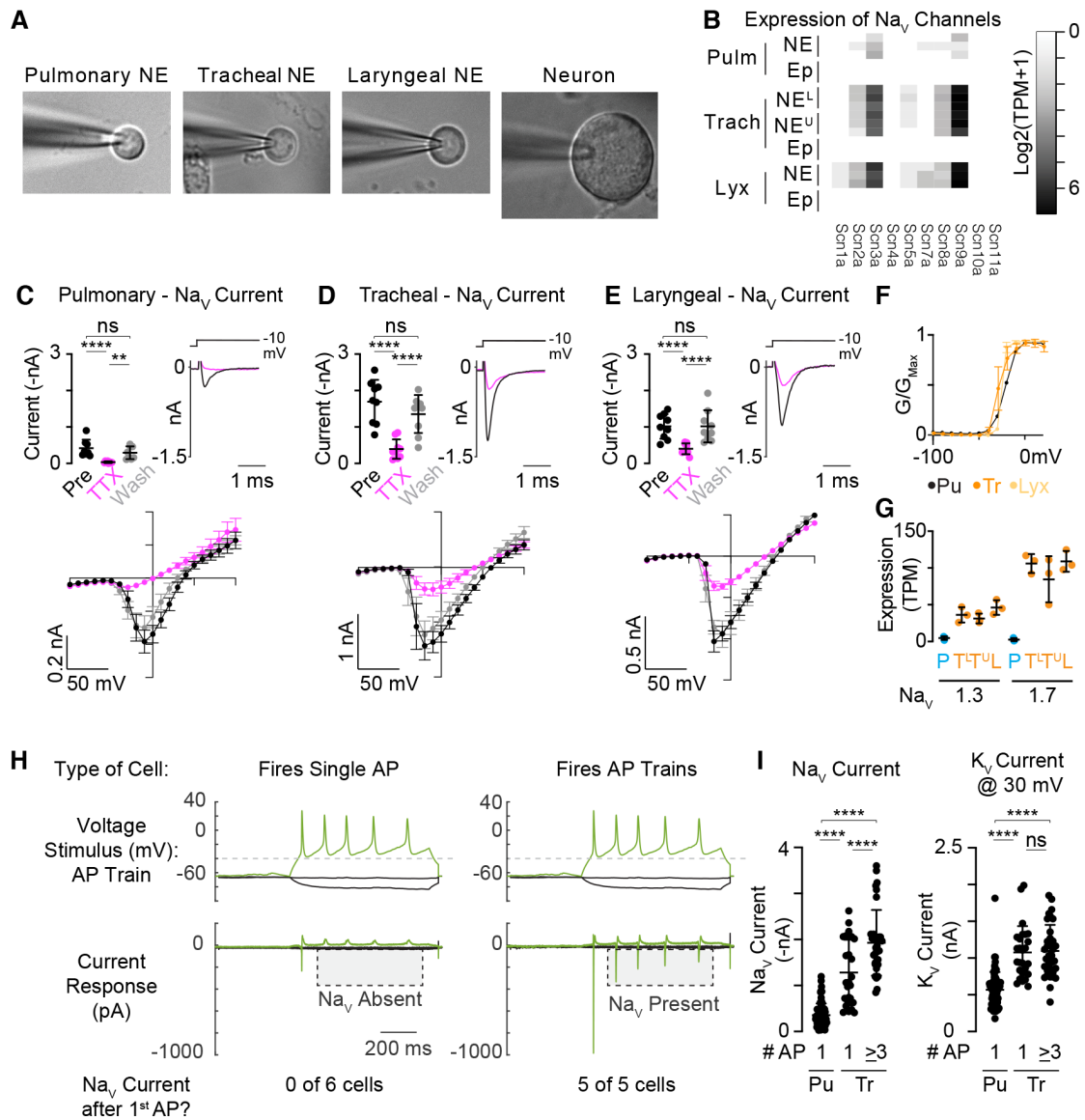0
AP 1 1 ≥3
Pu Tr
**** **** ns

Fig. S2. Tracheal and laryngeal NE cells have larger Na$_V$ currents. (**A**) Brightfield images of whole-cell patch-clamp electrophysiology with dissociated NE cells or a neuron. (**B**) Expression (Log2 transformed TPM+1) for voltage-gated sodium (Na$_V$) channel transcripts. Neuroendocrine (NE) and epithelial (Ep) cells from lung, trachea and larynx. NE^L and NE^U are lower and upper trachea, respectively. (**C-E**) Voltage-gated inward currents were inhibited by the Na$_V$ channel antagonist tetrodotoxin (TTX, 500 nM) in pulmonary (**C**), tracheal (**D**) and laryngeal (**E**) NE cells. Quantification (top left, negative nA), representative current response to -10 mV step (top right) and current-voltage relationship (bottom, mean ± SEM) of peak inward current for before (pre, black), during (TTX, pink) and after (wash, grey) application of TTX. Repeated measures one-way ANOVA ($P < 0.0001$ for all) and Tukey's multiple comparisons test. (**F**) NE cells had similar conductance-voltage (G/V) relationships for Na$_V$ channels. (**G**) Expression (TPM) of the two most highly expressed Na$_V$ transcripts (Na$_V$ 1.3 and 1.7) in pulmonary (P), lower tracheal (T^L), upper tracheal (T^U) and laryngeal (L) NE cells. (**H**) Measuring current responses to action potential play-back using patch-clamp electrophysiology. Tracheal NE cells were first phenotyped as being capable of firing single (left) or repetitive (right) action potentials in response to a small depolarizing current. Cells were then given a pre-recorded action potential train as a voltage stimulus (top) while measuring current responses (bottom). All cells that could fire AP trains had Na$_V$ current with each spike of the action potential train. Cells that fired a single AP had Na$_V$ current only with the first spike of the action potential train, suggesting they depleted their pool of available Na$_V$ current. $n = 5 - 6$ cells. (**I**) Na$_V$ and K$_V$ currents in pulmonary NE cells and tracheal NE cells that fired only 1 or more than 3 action potentials. Data are replotted/reanalyzed from Fig. 1G. One-way ANOVA ($P < 0.0001$ for all) and Holm-Sidak's multiple comparison test. * $P < 0.05$, ** $P < 0.01$, *** $P < 0.001$ and **** $P < 0.0001$. Data are represented as means ± SDs. See Table S1 for extended detail on statistics and P values.

Fig. S3.

A Pulmonary - K_V Current

B Tracheal - K_V Current

C Laryngeal - K_V Current

D

E

F Contribution of K_V Channels to Outward K Current in Tracheal NE Cells

Electrophysiological Signature of K2P

Order of Manipulation:
- External
- TEA/TTX (Most Na_V and K_V)
- TTX/4AP (K_V1-4)
- TTX/4AP/XE991 (K_V7)
- TTX/4AP/XE991/TEA
- TTX/4AP/XE991/TEA +140mM K (K2P)
- Wash

G

H Expression of K_V Channels

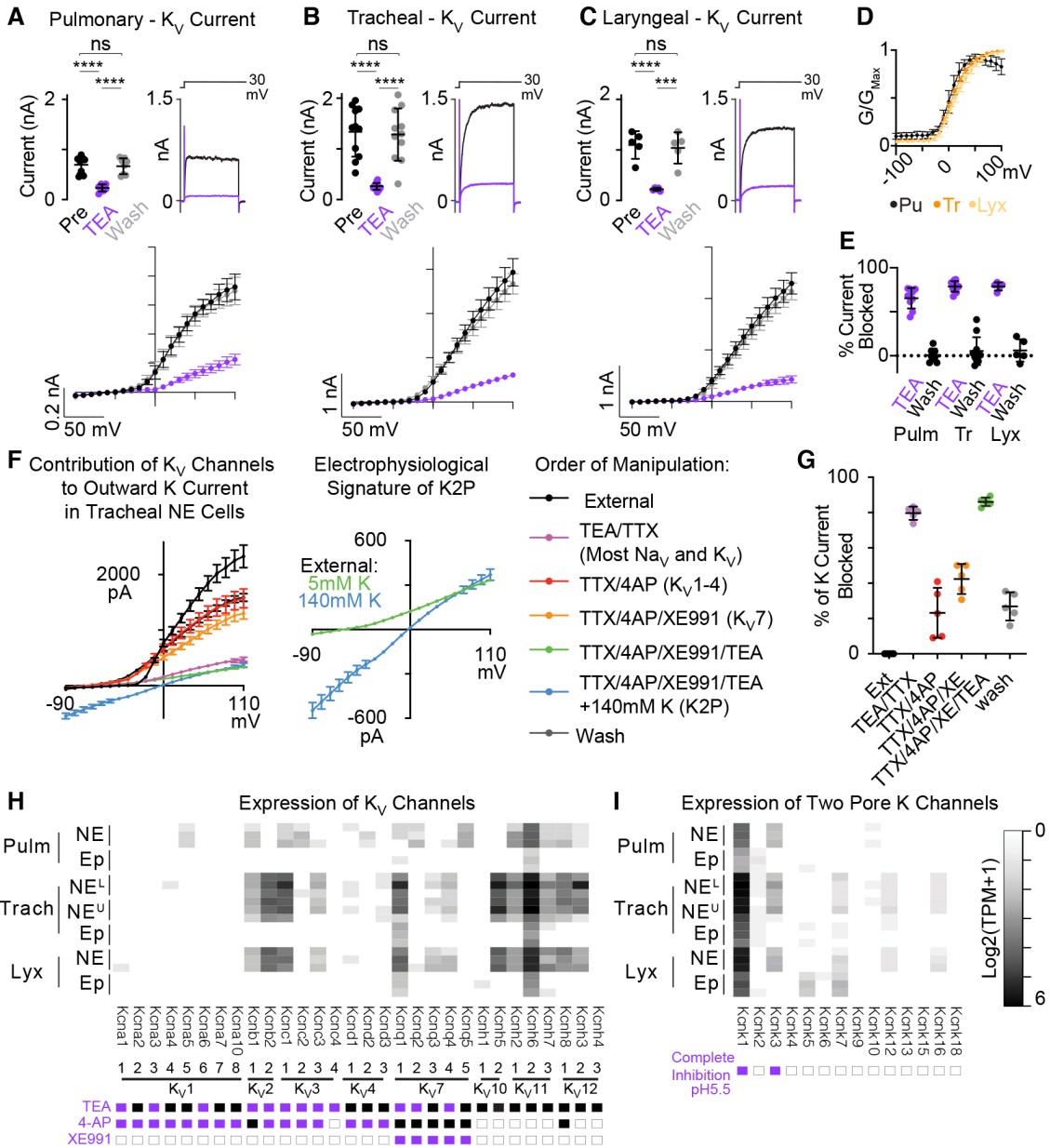**I** Expression of Two Pore K Channels

Fig. S3. Tracheal and laryngeal NE cells have larger K$_V$ currents. (**A-C**) Voltage-gated outward currents were inhibited by the K channel blocker TEA in pulmonary (**A**), tracheal (**B**) and laryngeal (**C**) NE cells. Quantification (top left, nA), representative current response to +30 mV step (top right) and current-voltage relationship (bottom, mean ± SEM) of mean outward current for before (pre, black), during (TEA, purple) and after (wash, grey) application of TEA. Repeated measures one-way ANOVA (*P* <0.0001 for all) and Tukey's multiple comparisons test. (**D**) NE cells had similar conductance-voltage (G/V) relationships for K channels. (**E**) Quantification of the percentage of outward potassium current blocked by TEA and wash. (**F**) Current-voltage relationship of mean outward potassium current (mean ± SEM). To isolate the contribution of various K channels we sequentially applied the following blockers with TTX present: 4AP (blocks K$_V$ 1-4), XE991 (blocks K$_V$ 7) and TEA (blocks K$_V$ 1-7). This demonstrates that there is a heterogeneous mixture of channels contributing to the K$_V$ current (left). In the presence of 4AP/XE991/TEA, which together fully block K$_V$ current, we shifted the external potassium concentration from 5 mM (green) to 140 mM (blue). In the presence of equimolar potassium inside/outside of the cell (140 mM), we observed that the K current became linear, which is characteristic of two pore potassium channels (right). (**G**) Quantification of percentage of outward potassium current blocked. (**H**, **I**) Expression (Log2 transformed TPM+1) of voltage-gated potassium (**H**) and two-pore potassium (**I**) channel transcripts (top). Neuroendocrine (NE) and epithelial (Ep) cells from lung, trachea and larynx. NE^L and NE^U are lower and upper trachea. Summary of known effects of the pharmacological blockers TEA, 4AP and XE991 and the physiological blocker pH 5.5 with purple squares indicating that the agent is known to inhibit the channel, black indicating it is known not to inhibit the channel, and white indicating that it has an uncharacterized effect at the concentrations used in panels **A-H**. * *P* < 0.05, ** *P* < 0.01, *** *P* < 0.001 and **** *P* < 0.0001. Data are represented as means ± SDs. See Table S1 for extended detail on statistics and P values.

Fig. S4.
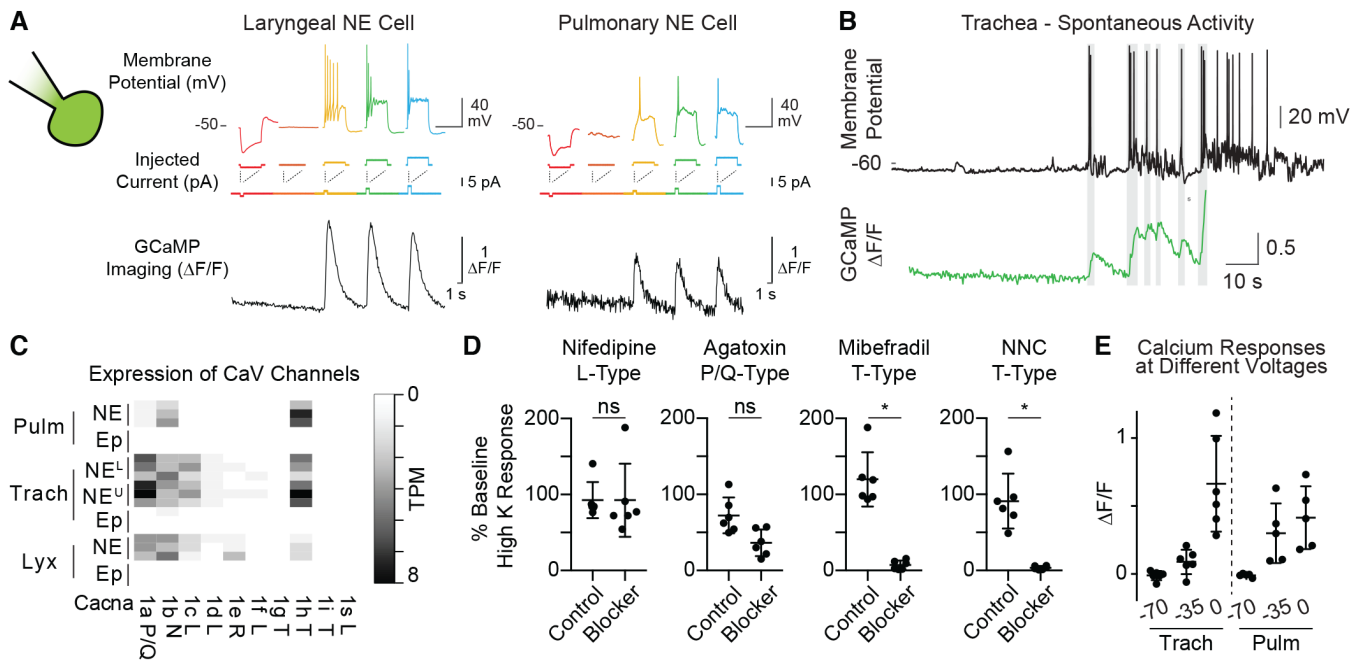
Fig. S4. Depolarization of airway NE cells leads to calcium influx through voltage-gated calcium channels. (**A**) Representative laryngeal and pulmonary NE patch-clamp electrophysiology-imaging traces. Current (middle) was injected into NE cell while recording membrane potential (top) and change in GCaMP fluorescence (bottom). (**B**) Representative patch-clamp electrophysiology-imaging trace of a spontaneously active tracheal NE cell with simultaneous recording of membrane potential (top) and GCaMP fluorescence (bottom). (**C**) Expression (TPM) of voltage-gated calcium channels. Neuroendocrine (NE) and epithelial (Ep) cells from lung, trachea and larynx. NE^L and NE^U are lower and upper trachea. (**D**) Quantification of effect of Ca_V antagonists on high-K-evoked calcium responses in tracheal NE cells. Baseline high-K was recorded, then external saline was perfused on the cell (control), followed by perfusion of the blocker. Ca_V blockers (μM): 10 nifedipine, 0.3 ω-agatoxin IVA, 5 mibefradil, and 10 NNC-55-0396. Wilcoxon signed rank test, $n = 6$, P = 0.69, 0.063, 0.031, 0.031, respectively. (**E**) Measuring change in GCaMP fluorescence of tracheal and pulmonary NE cells as cells are depolarized to either -70, -35 and 0 mV using an electrophysiology recording electrode. -70 mV is subthreshold for all Ca_V channels, -35 mV is above threshold for only T-type Ca_V channels and 0 mV is above threshold for almost all Ca_V channels. * $P < 0.05$, ** $P < 0.01$, *** $P < 0.001$ and **** $P < 0.0001$. Data are represented as means ± SDs. See Table S1 for extended detail on statistics and P values.

Fig. S5.

A

Expression of *Piezo2* Transcript

TPM (y-axis: 0, 30)

NE Epi | NE Low NE Up Epi | NE Epi
Pulm | Trach | Lyx

B Mechanosensitive Cells

Peak MS Current (-pA) (y-axis: 0, 1500)

Pulm Bronch Trach Lyx

\# MS cells: $\frac{10}{10}$ $\frac{3}{7}$ $\frac{1}{11}$ $\frac{1}{10}$

C

***

Min displacement for response (µm) (y-axis: 0, 10)

Pulm Br/Tr/Lyx

D

25 pA

Na_V Current (-pA) (y-axis: 2000)

Bronchial NE (Solitary)
Pulmonary NE (Clustered)

Piezo2 Current (-pA) (x-axis: 1500)

E Lung- Mechanically Evoked Activity

Stim

Membrane Potential -80

20 mV

GCaMP ΔF/F

0.1

10 s

F

Human Pulmonary NE Cells
Travaglini et al 2020
Average of 50 cells
2% of Epithelial Cells

p Value (y-axis: 10^{-100}, 10^{-50}, 10^0)

GRP
SCG2
SYT1 SCG3 DDC CALCA
KCNK3 KCNH6 ASCL
PCSKN1 CHGB
UCHL1 KCNJ6 TPH1
SYT7
SYT13 PIEZO2
SYT4
SNAP25
SCN3A
SYP CACNA1A

Average log(Fold Change) (x-axis: 0, 5, 10)

Human Tracheal NE Cells
Goldfarbmuren et al 2020
Average of 87 cells
0.25% of Epithelial Cells

p Value (y-axis: 10^{-300}, 10^{-200}, 10^{-100}, 10^0)

SCG3 CHGB
CHGA SCG2
CACNA1A PCSKN1 GRP
ASCL1 CALCA
TPH1 SYT1
DDC SUCNR1
SYT7 UCHL1
SNAP25
SYT13 KCNH6
SYT11 KCNJ6 SCN3A
SYP
OR51E1
TRPM8

Average log(Fold Change) (x-axis: 0, 2, 4, 6)

- ● NE genes
- ● Voltage Gated Channels
- ● Synaptic Proteins
- ● Receptors

Fig. S5. Mechanical sensitivity of pulmonary NE cells. (**A**) Expression (TPM) of the mechanosensitive cation channel *Piezo2* in NE and control epithelial (Ep) cells. (**B**) Quantification of peak inward mechano-evoked current for mechanically sensitive (MS) cells (top). Number of MS cells over the total number of cells recorded (bottom) for pulmonary (pulm), extra pulmonary bronchial (bronch), tracheal (trach) and laryngeal (lyx) NE cells. (**C**) Quantification of minimum displacement of mechanical probe needed to evoke a response in MS cells. Mann Whitney test ($P = 0.001$). (**D**) Relationship between Na_V current and mechanosensitive current in intrapulmonary pulmonary NE cells (blue) and extrapulmonary bronchial NE cells (red). (**E**) Simultaneous recording of changes in membrane potential (middle) and calcium influx (bottom) in response to mechanical stimulation (top). (**F**) Scatter plot of p value vs average log(Fold Change) for human pulmonary NE cells (left) and human tracheal NE cells (right) computationally identified in human single cell sequencing datasets from Travaglini *et al* 2020 and Goldfarbmuren *et al* 2020, respectively. Each dot is the average value for all identified NE cells compared to other non-NE epithelial cells for a given transcript. * $P < 0.05$, ** $P < 0.01$, *** $P < 0.001$ and **** $P < 0.0001$. Data are represented as means ± SDs. See Table S1 for extended detail on statistics and P values.
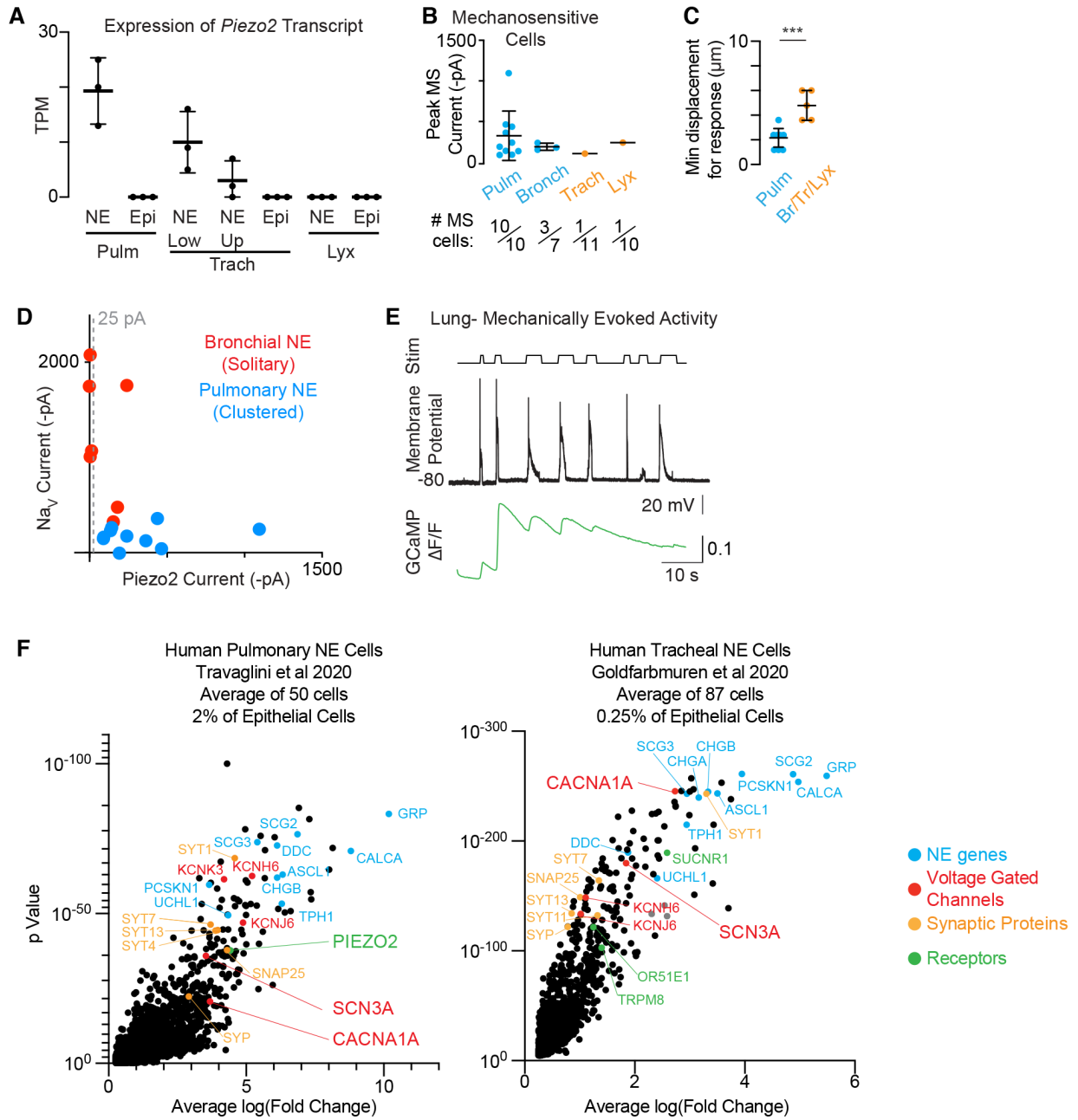
Fig. S6.

A $Ascl1^{CreERT2}; Polr2a^{LSL-GCaMP5G-t2a-tdTomato}$

B NE Cell Piezo2 KO: $Ascl1^{CreERT2}; Polr2a^{LSL-GCaMP5G-t2a-tdTomato}; Piezo2^{Flox/Flox}$

Pulmonary NE Cells   Tracheal NE Cells

C

D

Fig. S6. Water responses in airway NE cells. (**A**) GCaMP responses to perfusion of external saline, high potassium (HK) and water in pulmonary NE cell from precision cut lung slices. Representative images (left), representative trace (middle) and quantification of responses to stimuli (right). Repeated measures ANOVA ($P < 0.0001$) with Tukey's multiple comparisons test where different letters denote significant differences. (**B**) Representative images (top) and quantification (bottom) of GCaMP responses to external saline (S), water (W) and HK in dissociated pulmonary and tracheal NE cells from WT and *Piezo2*-KO animals. Repeated measures ANOVA (all $P < 0.01$) with Holm-Sidak's multiple comparison test to external saline. (**C**) Calcium responses to water (10 mOSM) and 300 mOSM solutions with (+) and without (-) 2 mM calcium. Repeated measures ANOVA ($P < 0.0001$) and Tukey's multiple comparisons test where different letters denote significant differences. (**D**) Simultaneous calcium imaging (green) and electrophysiological recording of membrane potential in response to different osmolarities. Only water lacks external sodium and potassium ions with osmolarity increased by mannitol. * $P < 0.05$, ** $P < 0.01$, *** $P < 0.001$ and **** $P < 0.0001$. Data are represented as means ± SDs. See Table S1 for extended detail on statistics and P values.
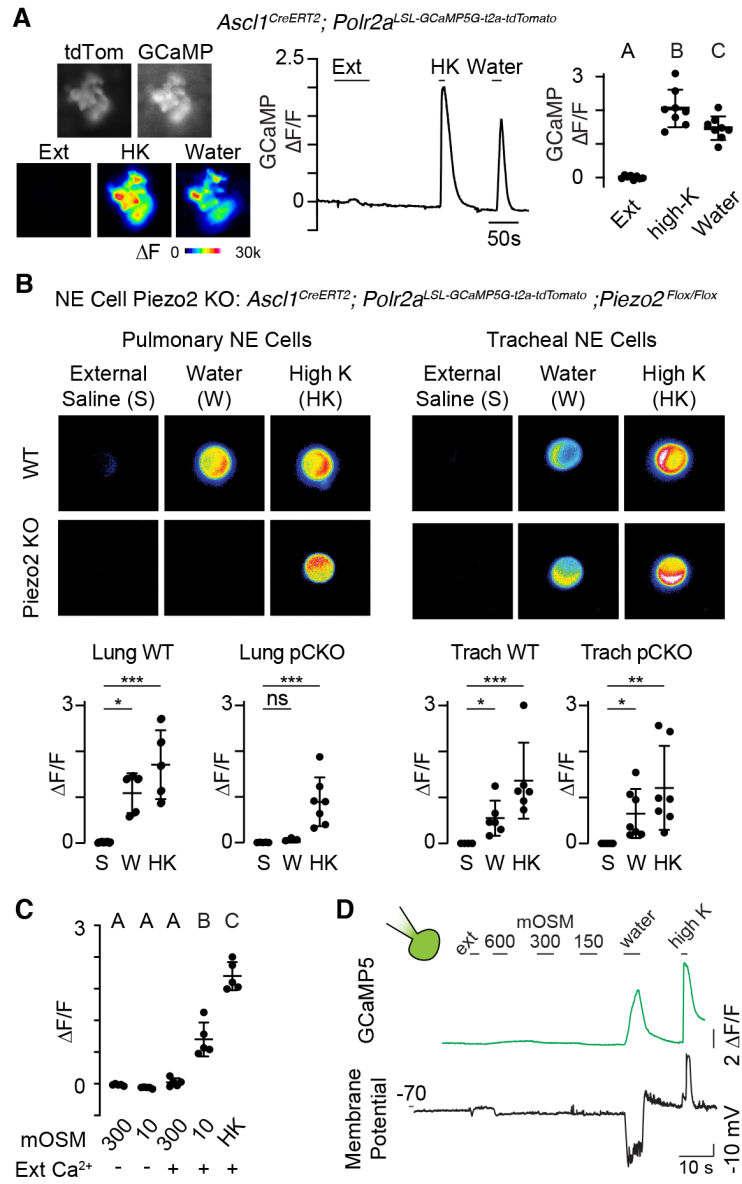
Fig. S7.
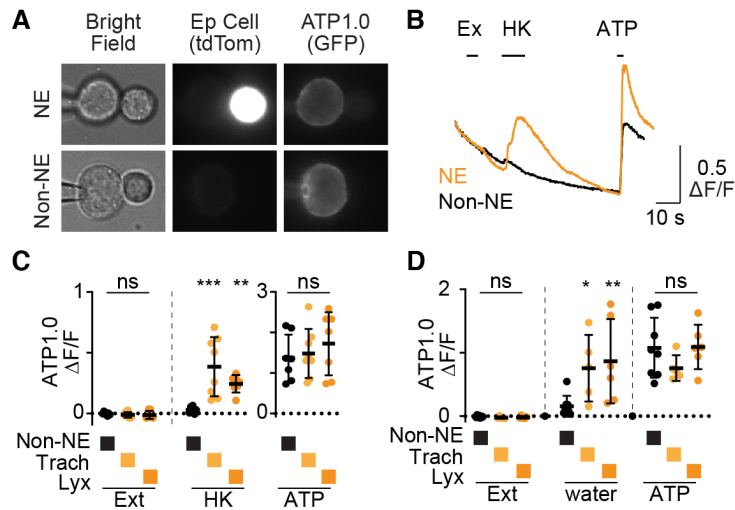
Fig. S7. Water and HK evoke ATP release from NE cells. (**A**) Representative brightfield (top), tdTomato fluorescence (middle) and GFP fluorescence (bottom) images of an ATP1.0-transfected HEK293T biosensor cell proximal to a NE cell or a non-NE cell. (**B**, **C**) Representative trace (**B**) and quantification (**C**) of change in ATP1.0 biosensor fluorescence in response to pulses of external saline (Ext), high potassium (HK) or 10 μM ATP applied to a NE cell (orange) or non-NE cell (black). Kruskal-Wallis test ($P = 0.3781$, < 0.0001 and 0.4452, respectively) with Dunn's multiple comparisons test to non-NE cell (right). (**D**) Quantification of change in fluorescence of ATP1.0 in response to pulses of external saline, water and ATP. Kruskal-Wallis test ($P = 0.3031$, 0.0025, 0.4452, respectively) with Dunn's multiple comparisons test to non-NE cell. * $P < 0.05$, ** $P < 0.01$, *** $P < 0.001$ and **** $P < 0.0001$. Data are represented as means ± SDs. See Table S1 for extended detail on statistics and P values.

Fig. S8.

A

Ascl1^CreERT2^; lsl-ChR2

Pgp9.5

ChR2-eYFP

B

On Lyx — SLN

On Trach — RLN

Ex vivo Recording Electrode

lsl-ReaChr

SLN — ns — RLN — ns

CAP/min

4000

0

Opto - +
On Lyx

800

0

- +
On Trach

C

Ascl1^CreERT2^; lsl-ChR2

Larynx Stimulation — SLN

Ex vivo Recording Electrode

High Salt — ns

#CAP/min

400

0

*Ascl1^CreERT2^*   +
lsl-ChR2   +   +

Optogenetic Activation — ***

#CAP/min

2000

0

*Ascl1^CreERT2^*   +
lsl-ChR2   +   +

D   Baseline Noise   High Salt   Optogenetic Activation

lsl-ChR2

Ascl1^CreERT2^; lsl-ChR2

E   *Ascl1^CreERT2^; lsl-ReaChR*   Stimulate: On Trach   Record: RLN

Basal

Saline

| 0.1 μV

Basal

PPADs

| 0.1 μV   20 s

Fraction of CAPs (Post/Baseline)

1

0

***

Control   PPADs

F   Baseline Noise   High Salt (650 mM Na⁺) Before PPADS   High Salt (650 mM Na⁺) After PPADS
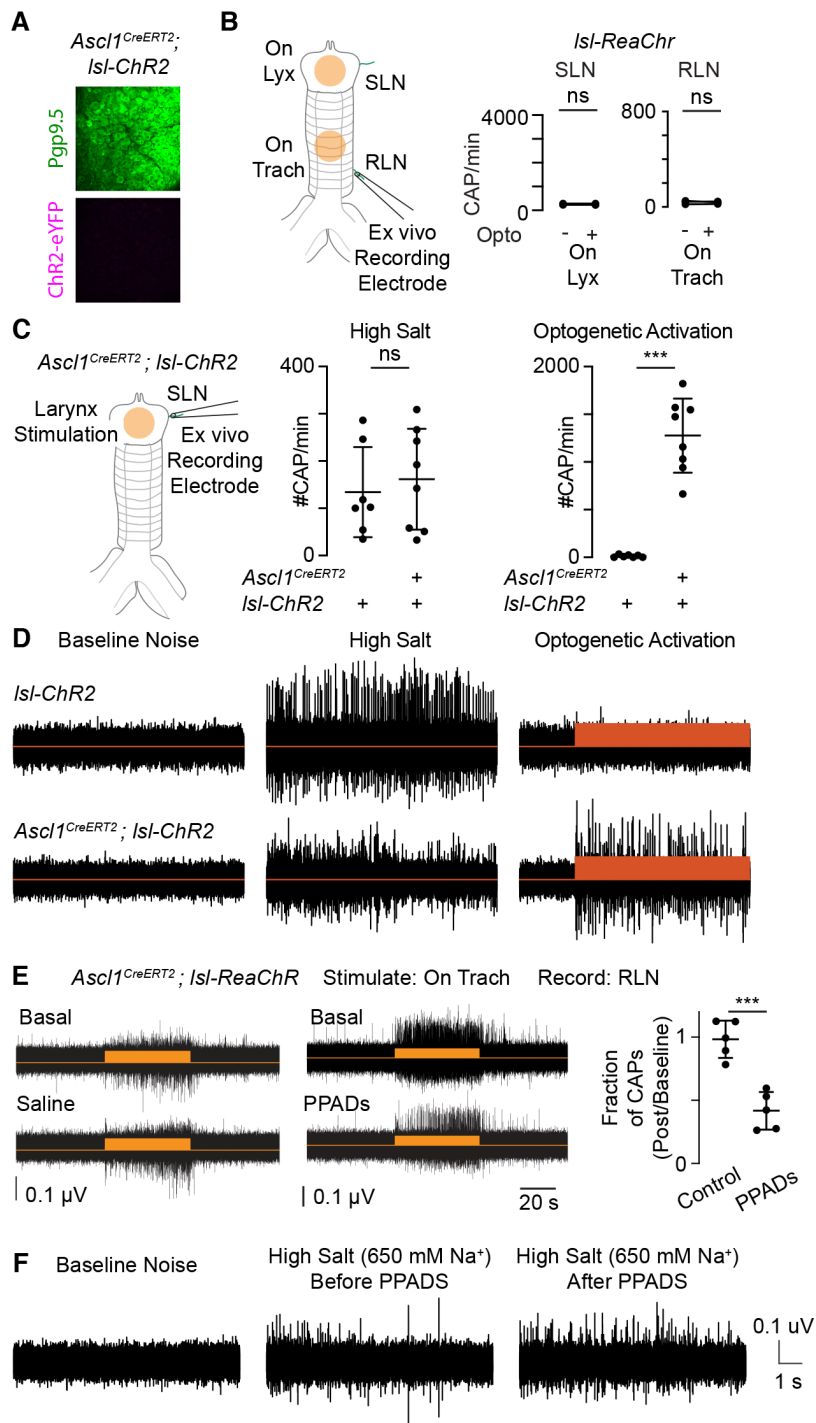
0.1 uV

1 s

Fig. S8. Optogenetic activation of tracheal and laryngeal NE cells drives activity in airway-innervating nerve fibers. (**A**) *Ascl1^{CreERT2}* does not express in vagal sensory neurons (green, PGP9.5+). Representative image of n = 5 mice using lsl-ChR2 and n = 5 mice lsl-tdTomato. (**B**) Schematic of *R26$^{lsl-ReaChR}$* control animal optogenetic explant preparation. Orange dots represent where light stimulation occurs (left). Number of compound action potentials (CAP) in the minute before (-) or during (+) optogenetic stimulation of larynx or trachea in *R26$^{lsl-ReaChR}$* control animals (right). Paired t-test (ns: *P > 0.05, n* = 4 preparations). (**C**) Schematic of experimental paradigm (left) and quantification of CAP rate in the superior laryngeal nerve (SLN) during stimulation with high salt solution (middle) or light to activate laryngeal NE cells (right). Mann-Whitney U test (*n* = 7-8, *P* = 0.7789*, P* = 0.0003). (**D**) Representative traces of baseline noise, application of high salt or optogenetic activation in control (lsl-ChR2) or experimental (*Ascl1^{CreERT2}; lsl-ChR2*) animals. (**E**) Effect of incubating the preparation in vehicle control (representative trace, left) or broad P2x receptor antagonist (PPADS, representative trace, middle) on optogenetics-induced activity in RLN. Quantification of fraction suppression (# Control or PPADs CAPS/# Basal CAPS), *n* = 5 preparations. Unpaired t-test, *P* = 0.0003. (**F**) Representative traces of baseline noise and application of high salt before or after incubation with PPADS. * *P* < 0.05, ** *P* < 0.01, and *** *P* < 0.001. Data are represented as means ± SDs. See Table S1 for extended detail on statistics and P-values.

Fig. S9.

A

Distribution of Peak Expirations

B

C

D
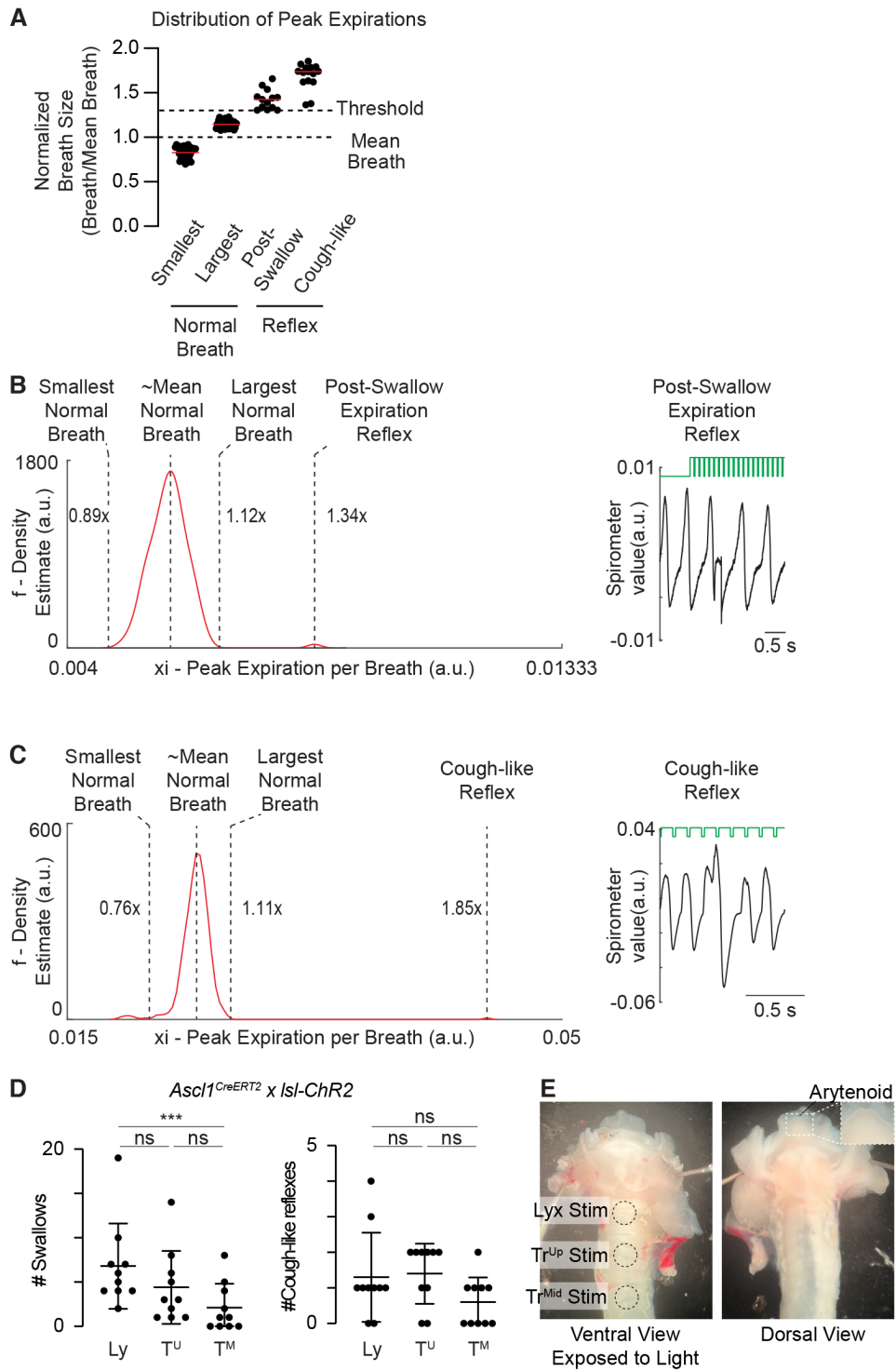
Ascl1^CreERT2 x lsl-ChR2

E

Fig. S9. Characteristics of post-swallow expiration and cough-like reflexes. (A-C) Characterizing reflexes using kernel density plots of distribution of peak expiratory flow (PEF) for each breath within a 1 min spirometry trace. (**A**) Smallest normal breath (left edge of normal breath distribution), largest normal breath (right edge of normal breath distribution), post-swallow expiration reflex breath and cough-like reflex breath expressed as fold change from mean PEF size for a given trace. (**B, C**) Representative kernel density plot (left) of a spirometry trace that contained a post-swallow expiration reflex (**B**) or cough-like reflex (**C**). PEF for most breaths fell within a narrow distribution, but the optogenetically-evoked reflexes were greater than 1.3x the size of the mean PEF for a given trace. (**D**) Number of swallows or cough-like reflexes when stimulating the larynx (Ly), upper trachea (T^U) or middle trachea (T^M) of ($Ascl1^{CreERT2}$; $lsl\text{-}ChR2$) mice. Data reanalyzed from Fig. 5F. Friedman test ($P = 0.0001$ and 0.016, respectively) with Dunn's multiple comparison test. (**E**) Excised airway tissue to show the approximate location of optogenetic stimulation on the ventral side relative to the taste-bud containing arytenoid tissue on the dorsal side. *** $P < 0.001$. Data are represented as means ± SDs. See Table S1 for extended detail on statistics and P values.
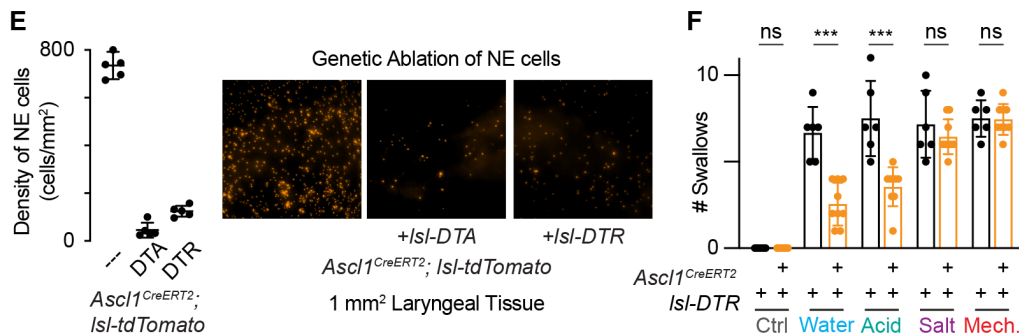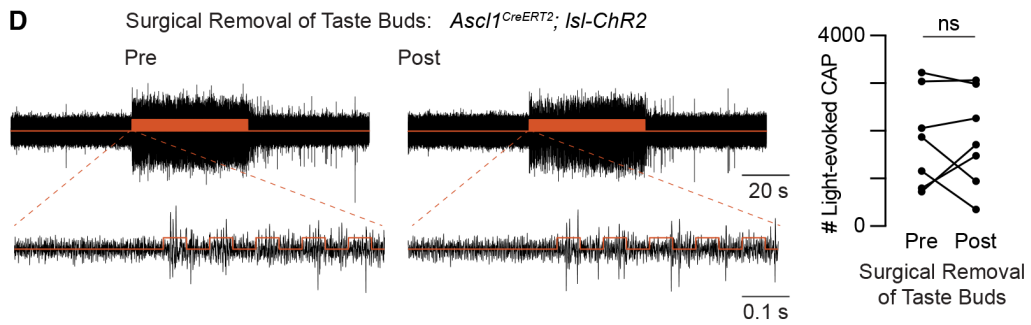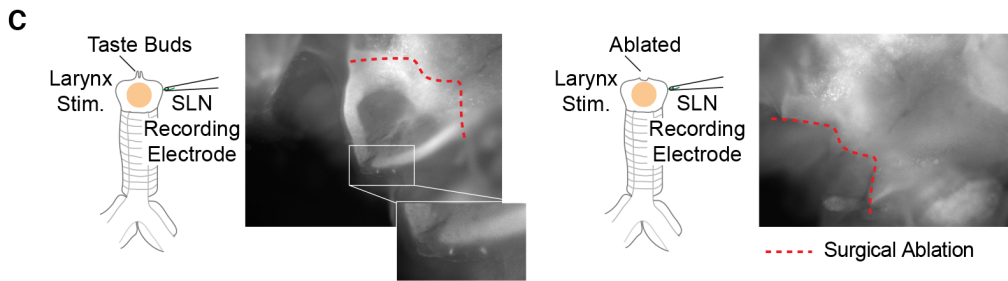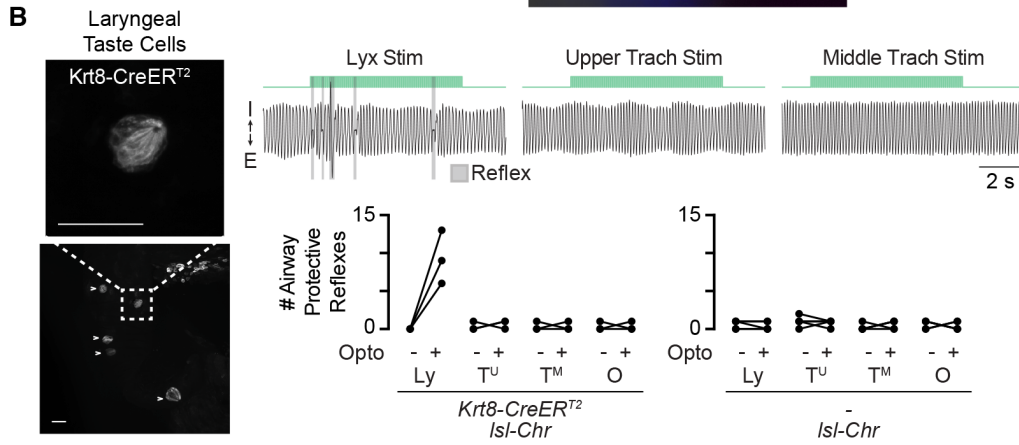
Fig. S10.

A

Ascl1^{CreERT2}; lsl-tdTomato

Krt8   tdTom   Pgp9.5

Laryngeal Taste Cells in the Arytenoid Folds

Ascl1^{CreERT2}; lsl-tdTomato

Taste Cells per Bud

Pgp+   Pgp+/Tdt+

B

Laryngeal Taste Cells

Krt8-CreER^{T2}

Lyx Stim   Upper Trach Stim   Middle Trach Stim

I ↑↓ E

Reflex   2 s

Airway Protective Reflexes

Opto - + - + - + - +   - + - + - + - +

      Ly T^U T^M O   Ly T^U T^M O

Krt8-CreER^{T2}   -
lsl-Chr   *lsl-Chr*

C

Taste Buds

Larynx Stim.   SLN Recording Electrode

Ablated

Larynx Stim.   SLN Recording Electrode

--- Surgical Ablation

D

Surgical Removal of Taste Buds: *Ascl1^{CreERT2}; lsl-ChR2*

Pre   Post

20 s

0.1 s

ns

Light-evoked CAP

Pre   Post

Surgical Removal of Taste Buds

E

Density of NE cells (cells/mm²)

--- DTA DTR

Ascl1^{CreERT2}; lsl-tdTomato

Genetic Ablation of NE cells

+lsl-DTA   +lsl-DTR

Ascl1^{CreERT2}; lsl-tdTomato

1 mm² Laryngeal Tissue

F

ns   ***   ***   ns   ns

Swallows

Ascl1^{CreERT2} + + + + + + + + + + +
lsl-DTR   + +   + +   + +   + +

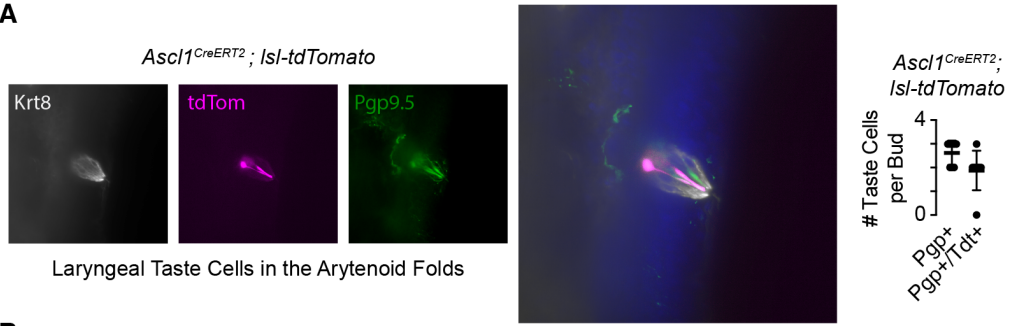Ctrl   Water   Acid   Salt   Mech.

Fig. S10. Details of taste cells and genetic ablation of NE cells. (**A**) $Ascl1^{CreERT2}$ labels a small subset of taste cells in the taste bud. Representative images (left) of all taste cell (Krt8+) with $Ascl1^{CreERT2}$ labeling Type III taste cells (Pgp9.5). Quantification (right) of number of taste cells that are tdTomato+ or double-positive for tdTomato/PGP9.5 within a given taste bud. Each dot represents # taste cells per taste bud pooled from 4 animals. (**B**) Representative image (left) of taste bud labeled by $Krt8$-$CreER^{T2}$; lsl-$ChR2$-YFP. Representative traces (right, top) and quantification (right, bottom) of airway protective reflexes following optogenetic stimulation of cells in the larynx (ly), upper trachea (T^U), mid-trachea (T^M) and off airway (O) for $Krt8$-$CreER^{T2}$; $R26^{lsl\text{-}ChR}$ and $R26^{lsl\text{-}ChR}$ animals (n = 3-5 animals). (**C**) Schematic and representative images of surgical ablation of arytenoid tissue. Images are of live tissue immediately before/after the experiment and were acquired using a GFP illumination/filter on a dissecting microscope. (**D**) Representative traces (left) and quantification (right) of light-evoked SLN activity before/after ablation. n = 7, Paired t-test. P = 0.9679. (**E**) Quantification (left) and representative images (right) of $Ascl1^{CreERT2}$; lsl-$tdTomato$+ NE cell density from DTA/DTR-neg animals ("---", data replotted from Fig. 1D), lsl-DTA positive animals and lsl-DTR positive animals that were also treated with diphtheria toxin. (**F**) Quantification of stimulus-evoked swallows in mice with NE cells ablated ($Ascl1^{CreERT2}$; lsl-DTR) and not ablated (lsl-DTR). All mice were treated with tamoxifen and diphtheria toxin in parallel. Mann-Whitney test (P > 0.999, = 0.0004, = 0.0004, = 0.5832 and = 0.964, respectively). *** P < 0.001. Data are represented as means ± SDs. See Table S1 for extended detail on statistics and P values. Scale bars are 50 μm.

Movie S1: Spontaneous bursts of calcium in tracheal NE cells. Imaging spontaneous calcium activity in NE cells (*Ascl1^{CreERT2}; Polr2a-GCaMP*) in tracheal explant preparations.

Movie S2: Optogenetic activation of laryngeal NE cells evokes visible swallowing

Movie S3: Optogenetic activation of upper tracheal NE cells evokes visible swallowing